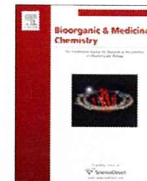


- 7) Ogawa M, Ishino S, Mukai T, et al. ^{18}F -FDG accumulation in atherosclerotic plaques: immunohistochemical and PET imaging study. *J Nucl Med.* 2004; 45: 1245-50.
- 8) Rudd JHF, Myers KS, Bansilal S, et al. ^{18}F Fluorodeoxyglucose positron emission tomography imaging of atherosclerotic plaque inflammation is highly reproducible. *J Am Coll Cardiol.* 2007; 50: 892-6.
- 9) Bural GG, Torigian DA, Chamroonrat W, et al. FDG-PET is an effective imaging modality to detect and quantify age-related atherosclerosis in large arteries. *Eur J Nucl Med Mol Imaging.* 2008; 35: 562-9.
- 10) Wykrzykowska J, Lehman S, Williams G, et al. Imaging of inflamed and vulnerable plaque in coronary arteries with ^{18}F -FDG PET/CT in patients with suppression of myocardial uptake using a low-carbohydrate, high-fat preparation. *J Nucl Med.* 2009; 50: 563-8.
- 11) Ogawa M, Magata Y, Kato T, et al. Application of [^{18}F]FDG-PET for monitoring the therapeutic effect of anti-inflammatory drugs on stabilization of vulnerable atherosclerotic plaques. *J Nucl Med.* 2006; 48: 1822-7.
- 12) Wu YW, Kao HL, Chen MF, et al. Characterization of plaques using ^{18}F -FDG PET/CT in patients with carotid atherosclerosis and correlation with matrix metalloproteinase-1. *J Nucl Med.* 2007; 48: 227-33.
- 13) Tahara N, Kai H, Yamagishi S, et al. Vascular inflammation evaluated by [^{18}F]fluorodeoxyglucose positron emission tomography is associated with the metabolic syndrome. *J Am Coll Cardiol.* 2007; 49: 1533-9.
- 14) Tahara N, Kai H, Ishibashi M, et al. Simvastatin attenuates plaque inflammation: evaluation by fluorodeoxyglucose positron emission tomography. *J Am Coll Cardiol.* 2006; 48: 1825-31.
- 15) Lee SJ, On YK, Lee EJ, et al. Reversal of vascular ^{18}F -FDG uptake with plasma high-density lipoprotein elevation by atherogenic risk reduction. *J Nucl Med.* 2008; 49: 1277-82.
- 16) Matter CM, Wyss MT, Meier P, et al. ^{18}F -Choline images murine atherosclerotic plaques ex vivo. *Arterioacler Thromb Vasc Biol.* 2006; 26: 584-9.
- 17) Ishino S, Mukai T, Kume N, et al. Lectin-like oxidized LDL receptor-1 (LOX-1) expression is associated with atherosclerotic plaque instability-analysis in hypercholesterolemic rabbits. *Atherosclerosis.* 2007; 195: 48-56.
- 18) Ishino S, Mukai T, Kuge Y, et al. Targeting of lectinlike oxidized low-density lipoprotein receptor 1 (LOX-1) with $^{99\text{m}}\text{Tc}$ -labeled anti-LOX-1 antibody: potential agent for imaging of vulnerable plaque. *J Nucl Med.* 2008; 49: 1677-85.
- 19) Li D, Patel A, Klivanov A, et al. Molecular imaging of atherosclerotic plaques targeted on oxidized LDL receptor LOX-1 using SPECT/CT and magnetic resonance [abstract]. *J Nucl Med.* 2009; 50: 657.
- 20) Sarai M, Hartung D, Petrov A, et al. Broad and specific caspase inhibitor-induced acute repression of apoptosis in atherosclerotic lesions evaluated by radiolabeled annexin A5 imaging. *J Am Coll Cardiol.* 2007; 50: 2305-12.
- 21) Laufer EM, Winkens MHM, Narula J, et al. Molecular imaging of macrophage cell death for the assessment of plaque vulnerability. *Arterioscler Thromb Vasc Biol.* 2009; 29: 1031-8.
- 22) Nguyen QD, Smith G, Glaser M, et al. Positron emission tomography imaging of drug-induced tumor apoptosis with a caspase-3/7 specific [^{18}F]labeled isatin sulfonamide. *Proc Natl Acad Sci U S A.* 2009; 106: 16375-80.
- 23) Ohshima S, Petrov A, Fujimoto S, et al. Molecular imaging of matrix metalloproteinase expression in atherosclerotic plaques of mice deficient in apolipoprotein E or low-density-lipoprotein receptor. *J Nucl Med.* 2009; 50: 612-7.
- 24) Zhang J, Nie L, Razavian M, et al. Molecular imaging of activated matrix metalloproteinase activity in the arterial wall in vivo. *Circulation.* 2008; 118: 1953-60.
- 25) Fujimoto S, Hartung D, Edward DS, et al. Molecular imaging of matrix metalloproteinase in atherosclerotic lesions: resolution with dietary modification and statin therapy. *J Am Coll Cardiol.* 2008; 52: 1847-57.
- 26) Tekabe Y, Qing L, Luma J, et al. Noninvasive monitoring the biology of atherosclerotic plaque development with radiolabeled annexin V and

- matrix metalloproteinase inhibitor in spontaneous atherosclerotic mice. *Circulation*. 2009; 120 Suppl : S365-6.
- 27) Kuge Y, Takai N, Ishino S, et al. Distribution profiles of membrane Type-1 Matrix Metalloproteinase (MT1-MMP), Matrix Metalloproteinase-2 (MMP-2) and cyclooxygenase-2 (COX-2) in rabbit atherosclerosis: comparison with plaque instability analysis. *Biol Pharm Bull*. 2007; 30: 1634-40.
- 28) Annovazz A, Bonanno E, Arca M, et al. ^{99m}Tc-interleukin-2 scintigraphy for the in vivo imaging of vulnerable atherosclerotic plaques. *Eur J Nucl Med Mol Imaging*. 2006; 33: 117-26.
- 29) Hartung D, Petrov A, Haider N, et al. Radio-labeled monocyte chemotactic protein 1 for the detection of inflammation in experimental atherosclerosis. *J Nucl Med*. 2007; 48: 1816-21.
- 30) van den Borne SWM, Isobe S, Verjans JW, et al. Molecular imaging of interstitial alterations in remodeling myocardium after myocardial infarction. *J Am Coll Cardiol*. 2008; 52: 2017-28.
- 31) Nahrendorf M, Zhang H, Hembrador S, et al. Nanoparticle PET-CT imaging of macrophages in inflammatory atherosclerosis. *Circulation*. 2008; 117: 379-87.
- 32) Cunningham CH, Arai T, Yang P, et al. Positive contrast magnetic resonance imaging of cells labeled with magnetic nanoparticles. *Magn Reson Med*. 2005; 53: 999-1005.
- 33) Dharmakumar R, Koktzoglou I, Li D. Generating positive contrast from off-resonant spins with steady-state free precession magnetic resonance imaging: theory and proof-of-principle experiments. *Phys Med Biol*. 2006; 51: 4201-15.
- 34) Mani V, Briley-Saebo KC, Itskovich VV, Set al. Gradient echo acquisition for superparamagnetic particles with positive contrast (GRASP) : sequence characterization in membrane and glass superparamagnetic iron oxide phantoms at 1.5T and 3T. *Magn Reson Med*. 2006; 55: 126-35.
- 35) Zurkiya O, Hu X. Off-resonance saturation as a means of generating contrast with superparamagnetic nanoparticles. *Magn Reson Med*. 2006; 56: 726-32.
- 36) Stuber M, Gilson WD, Schar M, et al. Positive contrast visualization of iron oxide-labeled stem cells using inversion-recovery with ON-resonant water suppression (IRON). *Magn Reson Med*. 2007; 58: 1072-7.
- 37) Korosoglou G, Tang L, Kedziorek D, et al. Positive contrast MR-lymphography using inversion recovery with ON-resonant water suppression (IRON). *J Magn Reson Imaging*. 2008; 27: 1175-80.
- 38) Korosoglou G, Weiss RG, Kedziorek DA, et al. Noninvasive detection of macrophage-rich atherosclerotic plaque in hyperlipidemic rabbits using "positive contrast" magnetic resonance imaging. *J Am Coll Cardiol*. 2008; 52: 483-91.
- 39) Winter P, Caruthers S, Zhang H, et al. Anti-angiogenic synergism of integrin-targeted fumagillin nanoparticles and atorvastatin in atherosclerosis. *J Am Coll Cardiol Imaging*. 2008; 1: 624-34.
- 40) Cyrus T, Zhang H, Allen JS, et al. Intramural delivery of rapamycin with alphavbeta3-targeted paramagnetic nanoparticles inhibits stenosis after balloon injury. *Arterioscler Thromb Vasc Biol*. 2008; 28: 820-6.



¹⁸F-labeled flavones for in vivo imaging of β -amyloid plaques in Alzheimer's brains

Masahiro Ono^{a,b,*}, Rumi Watanabe^a, Hidekazu Kawashima^c, Tomoki Kawai^b, Hiroyuki Watanabe^a, Mamoru Haratake^a, Hideo Saji^b, Morio Nakayama^{a,*}

^a Graduate School of Biomedical Sciences, Nagasaki University, 1-14 Bunkyo-machi, Nagasaki 852-8521, Japan

^b Graduate School of Pharmaceutical Sciences, Kyoto University, 46-29 Yoshida Shimoadachi-cho, Sakyo-ku, Kyoto 606-8501, Japan

^c Graduate School of Medicine, Kyoto University, Shogoin Kawahara-cho, Sakyo-ku, Kyoto 606-8507, Japan

ARTICLE INFO

Article history:

Received 10 December 2008

Revised 6 January 2009

Accepted 7 January 2009

Available online 20 January 2009

Keywords:

Alzheimer's disease

β -Amyloid plaque

PET

Flavone

ABSTRACT

In vivo imaging of β -amyloid ($A\beta$) aggregates in the brain may lead to early detection of Alzheimer's disease (AD) and monitoring of the progression and effectiveness of treatment. The purpose of this study was to develop novel ¹⁸F-labeled amyloid-imaging probes based on flavones as a core structure. Fluoropegylated (FPEG) flavone derivatives were designed and synthesized. The affinity of the derivatives for $A\beta$ aggregates varied from 5 to 321 nM. In brain sections of AD model mice, FPEG flavones with the dimethylamino group intensely stained β -amyloid plaques. In biodistribution experiments using normal mice, they displayed high uptake in the brain ranging from 2.9 to 4.2%ID/g at 2 min postinjection. The radioactivity washed out from the brain rapidly (1.3–2.0%ID/g at 30 min), which is highly desirable for β -amyloid imaging agents. FPEG flavones may be potential PET imaging agents for β -amyloid plaques in Alzheimer's brains.

© 2009 Elsevier Ltd. All rights reserved.

1. Introduction

Alzheimer's disease (AD) is a progressive neurodegenerative disorder characterized by cognitive decline, irreversible memory loss, disorientation, and language impairment. The presence of β -amyloid ($A\beta$) aggregates in the brain is generally accepted as a hallmark of AD.^{1,2} Since the only definitive diagnosis of AD is by pathological examination of postmortem staining of affected brain tissues, the development of techniques which enable one to image β -amyloid plaques in vivo has been strongly desired.^{3–5}

Recent success in developing radiolabeled agents targeting $A\beta$ aggregates has provided a window of opportunity to improve the diagnosis of AD. Preliminary reports of positron emission tomography (PET) imaging suggested that [¹¹C]4-*N*-methylamino-4'-hydroxystilbene (SB-13),^{6,7} [¹¹C] 2-(4'-(methylaminophenyl)-6-hydroxybenzothiazole (PIB),^{8,9} and [¹¹C]2-(2-[2-dimethylaminothiazol-5-yl]ethenyl)-6-(2-[fluoro]ethoxy)benzoxazole (BF-227)¹⁰ showed differential uptake and retention in the brain of AD patients as compared to controls. But ¹¹C is a positron-emitting isotope with a short $t_{1/2}$ (20 min), which limits its clinical application. Recent efforts have focused on the development of comparable agents labeled with a longer half-life isotope, ¹⁸F ($t_{1/2}$: 110 min). Preliminary

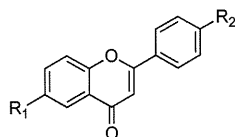
studies with [¹⁸F]-2-(1-(2-(*N*-(2-fluoroethyl)-*N*-methylamino)-naphthalen-6-yl)ethylidene)malononitrile ([¹⁸F]FDDNP)^{11,12} showed differential uptake and retention in the brain of AD patients for the first time. More recently, a stilbene derivative, [¹⁸F]BAY94-9172, has been shown to be useful for the imaging of β -amyloid plaques in living human brain tissue in clinical trials.¹³

To search for more candidates for ¹⁸F-labeled β -amyloid imaging agents for PET, we planned to evaluate a new series of flavone derivatives previously reported as useful for imaging β -amyloid by single photon emission computed tomography (SPECT).¹⁴ The derivatives showed good affinity for $A\beta$ aggregates in vitro in binding experiments using synthetic $A\beta$ aggregates and neuropathological staining of AD brain sections, suggesting these classes of radioiodinated flavones to be potential imaging agents.

Recently, Kung et al. exploited a novel approach by using fluoro-pegylation (FPEG) of the core structure for ¹⁸F labeling of derivatives.¹⁵ Since this approach offers a simple and easy way to incorporate ¹⁸F into the target without an appreciable increase in lipophilicity, we planned to apply it to the labeling of flavone derivatives. In addition to the structural characteristics of flavone as the pharmacophore, it has been shown that electron-donating groups such as amino, methylamino, dimethylamino, methoxy, or hydroxy groups play a critical role in the binding of $A\beta$ aggregates.^{6,8,16,17} With these considerations, we designed 12 fluorinated flavones with a fluorine or FPEGylation at position 4 and an electron-donating group at position 4' (Fig. 1).

* Corresponding authors. Tel.: +81 75 753 4608; fax: +81 75 753 4568 (M.O.); tel./fax: +81 95 819 2441 (M.N.).

E-mail addresses: ono@pharm.kyoto-u.ac.jp, mono@net.nagasaki-u.ac.jp (M. Ono), orio@nagasaki-u.ac.jp (M. Nakayama).



Compound	R ₁	R ₂
8a	FCH ₂ CH ₂ O	N(CH ₃) ₂
8b	F(CH ₂ CH ₂ O) ₂	N(CH ₃) ₂
8c	F(CH ₂ CH ₂ O) ₃	N(CH ₃) ₂
12	FCH ₂ CH ₂ O	NH ₂
13	FCH ₂ CH ₂ O	NHCH ₃
15b	F(CH ₂ CH ₂ O) ₂	NH ₂
15c	F(CH ₂ CH ₂ O) ₃	NH ₂
17b	F(CH ₂ CH ₂ O) ₂	NHCH ₃
17c	F(CH ₂ CH ₂ O) ₃	NHCH ₃
21	F	NH ₂
22	F	NHCH ₃
23	F	N(CH ₃) ₂

Figure 1. Chemical structure of FPEG-flavone derivatives.

We report here the *in vitro* and *in vivo* evaluation of a new series of flavone derivatives as agents for imaging β -amyloid with PET.

2. Experimental

All reagents were commercial products and used without further purification unless otherwise indicated. ¹H NMR spectra were obtained on a Varian Gemini 300 spectrometer with TMS as an internal standard. Coupling constants are reported in hertz. Multiplicity is defined by s (singlet), d (doublet), t (triplet), br (broad), and m (multiplet). Mass spectra were obtained on a JEOL IMS-DX instrument.

2.1. Chemistry

2.1.1. 4-Nitrobenzoic acid 2-acetyl-4-methoxyphenyl ester (1)

To a stirring solution of 4-nitrobenzoyl chloride (1.8 g, 10 mmol) in pyridine (20 mL) was added 2-hydroxy-5-methoxyacetophenone (1.6 g, 10 mmol). The reaction mixture was stirred at room temperature for 3 h, and poured into a 1 N aqueous HCl/ice solution with vigorous stirring. The precipitate that formed was filtered and washed with water to yield acetophenone **1** (2.9 g, 90.4% yield). ¹H NMR (300 MHz, CDCl₃) δ : 2.54 (s, 3H), 3.89 (s, 3H), 7.15–7.16 (m, 2H), 7.38 (d, *J* = 2.0 Hz, 1H), 8.37 (s, 4H).

2.1.2. 1-(5-Methoxy-2-hydroxyphenyl)-3-(4-nitrophenyl)propane-1,3-dione (2)

A solution of acetophenone **1** (2.9 g, 9.0 mmol) and pyridine (50 mL) was heated to 50 °C, and to it was added pulverized potassium hydroxide (2.5 g, 45.2 mmol). The reaction mixture was stirred for 90 min, and when it had cooled, 30 mL of 10% aqueous acetic acid solution was added. The yellow precipitate that formed was filtered to yield **2** (2.5 g, 88.1% yield). ¹H NMR (300 MHz, CDCl₃) δ : 3.85 (s, 3H), 6.84 (s, 1H), 6.99 (d, *J* = 6.9 Hz, 1H), 7.15–7.18 (m, 1H), 7.22 (d, *J* = 2.2 Hz, 1H), 8.10 (d, *J* = 6.6 Hz, 2H), 8.35 (d, *J* = 6.6 Hz, 2H), 11.5 (s, 1H).

2.1.3. 6-Methoxy-4'-nitroflavone (3)

A mixture of the diketone **2** (2.5 g, 8.0 mmol), concentrated sulfuric acid (2 mL), and glacial acetic acid (40 mL) was heated at 100 °C for 2 h and cooled to room temperature. The mixture was poured onto crushed ice, and the resulting precipitate was filtered to yield **3** (1.5 g, 63.5%). ¹H NMR (300 MHz, CDCl₃) δ : 3.93 (s, 3H), 6.92 (s, 1H), 7.31–7.37 (m, 1H), 7.54–7.61 (m, 2H), 8.11 (d, *J* = 9.3 Hz, 2H), 8.39 (d, *J* = 9.3 Hz, 2H).

2.1.4. 6-Methoxy-4'-aminoflavone (4)

A mixture of **3** (3.0 g, 10.2 mmol), SnCl₂ (7.6 g, 39.8 mmol), and EtOH (30 mL) was stirred under reflux for 40 min. After the mixture had cooled to room temperature, 1 M NaOH (50 mL) was added until the mixture became alkaline. After extraction with ethyl acetate, the combined organic layers were washed with brine, dried over Na₂SO₄, and filtered. The solvent was removed, and the residue was purified by silica gel chromatography (hexane/ethyl acetate = 1:2) to give 1.3 g of **4** (65.3% yield). ¹H NMR (300 MHz, CDCl₃) δ : 3.91 (s, 3H), 4.11 (s, broad, 2H), 6.69 (s, 1H), 6.75 (d, *J* = 6.6 Hz, 2H), 7.24–7.27 (m, 1H), 7.47 (d, *J* = 6.6 Hz, 1H), 7.59 (d, *J* = 2.2 Hz, 1H), 7.75 (d, *J* = 6.6 Hz, 2H).

2.1.5. 6-Methoxy-4'-dimethylaminoflavone (5)

To a mixture of **4** (401 mg, 1.5 mmol) and paraformaldehyde (450 mg, 15 mmol) in AcOH (10 mL) was added NaCNBH₃ (471 mg, 7.5 mmol) in one portion at room temperature. The resulting mixture was stirred at room temperature for 1.5 h, and the addition of 1 M NaOH was followed by extraction with CH₂Cl₂. The organic phase was dried over Na₂SO₄. The solvent was removed, and the residue was purified by silica gel chromatography (CHCl₃/MeOH = 20:1) to give 371 mg of **5** (83.7% yield). ¹H NMR (300 MHz, CDCl₃) δ : 3.07 (s, 6H), 3.91 (s, 3H), 6.70 (s, 1H), 6.75 (d, *J* = 9.0 Hz, 2H), 7.24–7.26 (m, 1H), 7.47 (d, *J* = 9.0 Hz, 1H), 7.59 (d, *J* = 2.2 Hz, 1H), 7.81 (d, *J* = 9.0 Hz, 2H).

2.1.6. 6-Hydroxy-4'-dimethylaminoflavone (6)

To a solution of **5** (371 mg, 1.5 mmol) in CH₂Cl₂ (10 mL) at 10 °C was added BBr₃ (7.5 mL, 1 M solution in CH₂Cl₂) dropwise in an ice bath. The mixture was allowed to warm to room temperature and was stirred for 12 h. Water was added while the reaction mixture was cooled in an ice bath to keep the reaction temperature at 0 °C. After extraction with CH₂Cl₂, the combined organic phase was dried over Na₂SO₄. The filtrate was concentrated and the residue was purified by silica gel chromatography (CHCl₃/MeOH = 20:1) to give 303 mg of **6** (71.8% yield). ¹H NMR (300 MHz, CDCl₃) δ : 3.05 (s, 6H), 6.74 (d, *J* = 9.3 Hz, 2H), 7.26 (d, *J* = 3.0 Hz, 1H), 7.45 (d, *J* = 9.0 Hz, 1H), 7.58 (d, *J* = 3.0 Hz, 1H), 7.77 (d, *J* = 9.0 Hz, 2H).

2.1.7. 6-Hydroxyethoxy-4'-dimethylaminoflavone (7a)

To a solution of **6** (85 mg, 0.30 mmol) and ethylene chlorohydrin (100 μ L, 1.50 mmol) in DMSO (3 mL) was added anhydrous K₂CO₃ (41 mg, 0.90 mmol). The reaction mixture was stirred at 120 °C for 48 h, then poured into water. After extraction with chloroform, the organic layers were combined and dried over Na₂SO₄. Evaporation of the solvent afforded a residue, which was purified by silica gel chromatography (CHCl₃/MeOH = 33:1) to give 30 mg of **7a** (30.5%). ¹H NMR (300 MHz, CDCl₃) δ : 3.06 (s, 6H), 3.98–4.05 (m, 2H), 4.17–4.23 (m, 2H), 6.69 (s, 1H), 6.76 (d, *J* = 9.3 Hz, 2H), 7.28 (d, *J* = 3.0 Hz, 1H), 7.47 (d, *J* = 9.0 Hz, 1H), 7.60 (d, *J* = 3.0 Hz, 1H), 7.80 (d, *J* = 9.0 Hz, 2H).

2.1.8. 6-(2-(2-Hydroxy-ethoxy)-ethoxy)-4'-dimethylaminoflavone (7b)

To a solution of **6** (82 mg, 0.29 mmol) and ethylene glycol mono-2-chloroethyl ether (37 μ L, 0.35 mmol) in DMF (3 mL) was added anhydrous K₂CO₃ (120 mg, 0.87 mmol). The reaction mixture was stirred at 120 °C for 11 h, then poured into water. After extraction with chloroform, the organic layers were combined and dried over Na₂SO₄. Evaporation of the solvent afforded a residue, which was purified by silica gel chromatography (hexane/ethyl acetate = 10:1) to give 107 mg of **7b** (99.3%). ¹H NMR (300 MHz, CDCl₃) δ : 3.07 (s, 6H), 3.69 (t, *J* = 5.1 Hz, 2H), 3.79 (s, 2H), 3.91 (t, *J* = 4.5 Hz, 2H), 4.26 (t, *J* = 4.5 Hz, 2H), 6.69 (s, 1H), 6.75 (d, *J* = 9.0 Hz, 2H), 7.27–7.30 (m, 1H), 7.47 (d, *J* = 9.0 Hz, 1H), 7.64 (d, *J* = 2.2, 1H), 7.81 (d, *J* = 9.0 Hz, 2H).

2.1.9. 6-(2-(2-(2-Hydroxy-ethoxy)-ethoxy)ethoxy)-4'-dimethylaminoflavone (7c)

To a solution of **6** (100 mg, 0.36 mmol) and 2-[2-(2-chloroethoxy)ethoxy]ethanol (62 μ L, 0.43 mmol) in DMF (3 mL) was added anhydrous K_2CO_3 (148 mg, 1.07 mmol). The reaction mixture was stirred at 120 °C for 17 h, then poured into water. After extraction with chloroform, the organic layers were combined and dried over Na_2SO_4 . Evaporation of the solvent afforded a residue, which was purified by preparative TLC ($CHCl_3/MeOH = 20:1$) to give 76 mg of **7c** (51.1%). 1H NMR (300 MHz, $CDCl_3$) δ : 3.07 (s, 6H), 3.62–3.76 (m, 8H), 3.91 (t, $J = 4.5$ Hz, 2H), 4.26 (t, $J = 4.5$ Hz, 2H), 6.69 (s, 1H), 6.77 (d, $J = 9.3$ Hz, 2H), 7.28–7.33 (m, 1H), 7.47 (d, $J = 9.0$ Hz, 1H), 7.60 (d, $J = 2.2$, 1H), 7.81 (d, $J = 9.0$ Hz, 2H).

2.1.10. 6-Fluoroethoxy-4'-dimethylaminoflavone (8a)

To a solution of **7a** (30 mg, 0.09 mmol) in ethylene glycol dimethyl ether (3 mL) was added dimethylamino sulfur trifluoride (DAST) (30 μ L, 0.23 mmol) in a dry ice-acetone bath. The reaction mixture was stirred for 6 h at room temperature. The mixture was then poured into a saturated $NaHSO_3$ solution and after extraction with chloroform, the organic phase was separated, dried over Na_2SO_4 , and filtered. The residue was purified by silica gel chromatography (hexane/ethyl acetate = 2:1) to give 16 mg of **8a** (53.0%). 1H NMR (300 MHz, $CDCl_3$) δ : 2.93 (s, 6H), 4.26–4.40 (m, 2H), 4.70–4.92 (m, 2H), 6.71 (s, 1H), 6.76 (d, $J = 9.0$ Hz, 2H), 7.29–7.35 (m, 1H), 7.50 (d, $J = 9.0$ Hz, 1H), 7.59 (d, $J = 3.3$ Hz, 1H), 7.82 (d, $J = 9.3$ Hz, 2H). EI-MS m/z 327 (M^+).

2.1.11. 6-(2-(2-Fluoro-ethoxy)-ethoxy)-4'-dimethylaminoflavone (8b)

To a solution of **7b** (29 mg, 0.08 mmol) in 1,2-dimethoxyethane (DME) (5 mL) was added DAST (21 μ L, 0.16 mmol) in a dry ice-acetone bath. The reaction mixture was stirred for 1.5 h at room temperature. The mixture was then poured into a saturated $NaHSO_3$ solution and after extraction with chloroform, after the organic phase was separated, dried over Na_2SO_4 , and filtered. The residue was purified by preparative TLC ($CHCl_3/MeOH = 20:1$) to give 15 mg of **8b** (51.5%). 1H NMR (300 MHz, $CDCl_3$) δ : 3.07 (s, 6H), 3.79 (t, $J = 4.2$ Hz, 1H), 3.89–3.96 (m, 3H), 4.26 (t, $J = 4.8$ Hz, 2H), 4.54 (t, $J = 4.2$ Hz), 4.69 (t, $J = 4.2$ Hz), 6.70 (s, 1H), 6.76 (d, $J = 9.0$ Hz, 2H), 7.27–7.33 (m, 1H), 7.49 (d, $J = 9.3$ Hz, 1H), 7.59 (d, $J = 3.0$, 1H), 7.81 (d, $J = 9.0$ Hz, 2H). EI-MS m/z 371 (M^+).

2.1.12. 6-(2-(2-(2-Fluoro-ethoxy)-ethoxy)ethoxy)-4'-dimethylaminoflavone (8c)

To a solution of **7c** (141 mg, 0.34 mmol) in DME (5 mL) was added DAST (90 μ L, 0.68 mmol) in a dry ice-acetone bath. The reaction mixture was stirred for 1 h at room temperature. The mixture was then poured into saturated $NaHSO_3$ solution and extracted with chloroform. After the organic phase was separated, dried over Na_2SO_4 and filtered, the residue was purified by preparative TLC (hexane/ethyl acetate = 1:5) to give 21 mg of **8c** (14.9%). 1H NMR ($CDCl_3$) δ : 3.08 (s, 6H), 3.69–3.81 (m, 6H), 3.91 (t, $J = 4.8$ Hz, 2H), 4.24 (t, $J = 4.8$ Hz, 2H), 4.49 (t, $J = 4.5$ Hz, 1H), 4.65 (t, $J = 4.5$ Hz, 1H), 6.69 (s, 1H), 6.76 (d, $J = 9.0$ Hz, 2H), 7.27–7.33 (m, 1H), 7.48 (d, $J = 9.0$ Hz, 1H), 7.59 (d, $J = 2.2$, 1H), 7.81 (d, $J = 9.0$ Hz, 2H). EI-MS m/z 415 (M^+).

2.1.13. 6-Hydroxy-4'-nitroflavone (9)

The same reaction as described above to prepare **6** was used, and 560 mg of **9** was obtained from **3** and BBr_3 . EI-MS m/z 283 (M^+).

2.1.14. 6-(2-Hydroxy-ethoxy)-4'-nitroflavone (10a)

The same reaction as described above to prepare **7a** was used, and 40 mg of **10a** was obtained from **9** in a yield of 9.9%. 1H

NMR (300 MHz, $CDCl_3$) δ : 3.88–4.02 (m, 2H), 4.13–4.20 (m, 2H), 6.89 (s, 1H), 7.38–7.41 (m, 1H), 7.59 (d, $J = 9.3$ Hz, 1H), 7.67 (d, $J = 3.3$ Hz, 1H), 8.12 (d, $J = 9.0$ Hz, 2H), 8.46 (d, $J = 9.0$ Hz, 2H).

2.1.15. 6-(2-(2-Hydroxy-ethoxy)-ethoxy)-4'-nitroflavone (10b)

The same reaction as described above to prepare **7b** was used, and 830 mg of **10b** was obtained from **9**. 1H NMR (300 MHz, $CDCl_3$) δ : 3.70 (t, $J = 5.1$ Hz, 2H), 3.79 (s, 2H), 3.93 (t, $J = 5.0$ Hz, 2H), 4.28 (t, $J = 4.8$ Hz, 2H), 6.90 (s, 1H), 7.37–7.41 (m, 1H), 7.56 (d, $J = 9.3$ Hz, 1H), 7.66 (d, $J = 3.3$ Hz, 1H), 8.10 (d, $J = 9.0$ Hz, 2H), 8.40 (d, $J = 9.0$ Hz, 2H).

2.1.16. 6-(2-(2-(2-Hydroxy-ethoxy)-ethoxy)ethoxy)-4'-nitroflavone (10c)

The same reaction as described above to prepare **7c** was used, and **10c** was obtained from **9** in a yield of 83.1%. 1H NMR (300 MHz, $CDCl_3$) δ : 3.64 (t, $J = 4.5$ Hz, 2H), 3.71–3.78 (m, 6H), 3.93 (t, $J = 4.8$ Hz, 2H), 4.27 (t, $J = 4.5$ Hz, 2H), 6.90 (s, 1H), 7.38–7.42 (m, 1H), 7.55 (d, $J = 9.0$ Hz, 1H), 7.61 (d, $J = 3.1$ Hz, 1H), 8.10 (d, $J = 8.7$ Hz, 2H), 8.39 (d, $J = 8.7$ Hz, 2H). EI-MS m/z 415 (M^+).

2.1.17. 6-(2-Fluoro-ethoxy)-4'-nitroflavone (11)

The same reaction as described above to prepare **8a** was used, and 24 mg of **11** was obtained from **10a** in a yield of 41.6%. 1H NMR (300 MHz, $CDCl_3$) δ : 4.26–4.41 (m, 2H), 4.71–4.92 (m, 2H), 6.91 (s, 1H), 7.42–7.44 (m, 1H), 7.56–7.61 (m, 2H), 8.11 (d, $J = 9.0$ Hz, 2H), 8.39 (d, $J = 9.3$ Hz, 2H).

2.1.18. 6-(2-Fluoro-ethoxy)-4'-aminoflavone (12)

The same reaction as described above to prepare **4** was used, and 22 mg of **12** was obtained from **11** in a yield of 41.6%. 1H NMR (300 MHz, $CDCl_3$) δ : 4.10 (s, 2H), 4.27–4.39 (m, 2H), 4.71–4.88 (m, 2H), 6.70 (s, 1H), 6.76 (d, $J = 9.0$ Hz, 2H), 7.29–7.35 (m, 1H), 7.49 (d, $J = 9.3$ Hz, 1H), 7.58 (s, 1H), 7.75 (d, $J = 9.0$ Hz, 2H). EI-MS m/z 299 (M^+).

2.1.19. 6-(2-Fluoro-ethoxy)-4'-methylaminoflavone (13)

To a solution of **12** (22 mg, 0.07 mmol) in DMSO (2 mL) were added methyl iodide (0.14 mL) and K_2CO_3 (50.8 mg, 0.37 mmol). The reaction mixture was stirred at room temperature for 5 h, and poured into water (30 mL). After extraction with ethyl acetate (2 \times 30 mL), the organic layers were combined and dried over Na_2SO_4 . Evaporation of the solvent afforded a residue, which was purified by reversed phase HPLC (acetonitrile/ $H_2O = 3:2$) to give 10 mg of **13** (43.4% yield). 1H NMR (300 MHz, $CDCl_3$) δ : 2.93 (s, 3H), 4.22 (s, 1H), 4.26–4.40 (m, 2H), 4.70–4.91 (m, 2H), 6.71 (s, 1H), 6.76 (d, $J = 9.0$ Hz, 2H), 7.29–7.35 (m, 1H), 7.50 (d, $J = 9.3$ Hz, 1H), 7.58 (s, 1H), 7.78 (d, $J = 8.7$ Hz, 2H). EI-MS m/z 313 (M^+).

2.1.20. 6-(2-(2-Hydroxy-ethoxy)-ethoxy)-4'-aminoflavone (14b)

The same reaction as described above to prepare **4** was used, and 251 mg of **14b** was obtained from **10b** in a yield of 37.9%. 1H NMR ($CDCl_3$) δ : 3.69 (t, $J = 5.1$ Hz, 2H), 3.79 (s, 2H), 3.91 (t, $J = 4.5$ Hz, 2H), 4.09 (s, 2H), 4.27 (t, $J = 4.2$ Hz, 2H), 6.69 (s, 1H), 6.76 (d, $J = 8.7$ Hz, 2H), 7.27–7.32 (m, 1H), 7.48 (d, $J = 9.3$ Hz, 1H), 7.65 (d, $J = 3.0$ Hz, 1H), 7.75 (d, $J = 8.4$ Hz, 2H). EI-MS m/z 387 (M^+).

2.1.21. 6-(2-(2-(2-Hydroxy-ethoxy)-ethoxy)ethoxy)-4'-aminoflavone (14c)

The same reaction as described above to prepare **4** was used, and 553 mg of **14c** was obtained from **10c** in a yield of 58.8%. 1H NMR (300 MHz, $CDCl_3$) δ : 3.62–3.65 (m, 2H), 3.71–3.78 (m, 6H), 3.91 (t, $J = 4.8$ Hz, 2H), 4.11 (s, 2H), 4.25 (t, $J = 4.5$ Hz, 2H), 6.68 (s, 1H), 6.75 (d, $J = 8.7$ Hz, 2H), 7.27–7.32 (m, 1H), 7.50 (d, $J = 9.0$ Hz, 1H), 7.59 (d, $J = 2.2$ Hz, 1H), 7.74 (d, $J = 8.7$ Hz, 2H). EI-MS m/z 387 (M^+).

2.1.22. 6-(2-(2-Fluoro-ethoxy)-ethoxy)-4'-aminoflavone (15b)

The same reaction as described above to prepare **8b** was used, and 10 mg of **15b** was obtained from **14b** in a yield of 9.1%. ¹H NMR (CDCl₃) δ: 3.79 (t, *J* = 4.2 Hz, 1H), 3.86–3.95 (m, 3H), 4.11 (s, 2H), 4.25 (t, *J* = 4.5 Hz, 2H), 4.53 (t, *J* = 4.2 Hz, 1H), 4.70 (t, *J* = 4.2 Hz, 1H), 6.68 (s, 1H), 6.75 (d, *J* = 9.0 Hz, 2H), 7.28–7.33 (m, 1H), 7.47 (d, *J* = 9.0 Hz, 1H), 7.58 (d, *J* = 3.0 Hz, 1H), 7.74 (d, *J* = 8.4 Hz, 2H). EI-MS *m/z* 343 (M⁺).

2.1.23. 6-(2-(2-(2-Fluoro-ethoxy)-ethoxy)ethoxy)-4'-aminoflavone (15c)

The same reaction as described above to prepare **8** was used, and 85 mg of **15c** was obtained from **14** in a yield of 81.3%. ¹H NMR (CDCl₃) δ: 3.62–3.65 (m, 2H), 3.70–3.78 (m, 7H), 3.82 (t, *J* = 3.9 Hz, 1H), 3.90 (t, *J* = 4.5 Hz, 2H), 4.22 (t, *J* = 4.5 Hz, 2H), 4.49 (t, *J* = 4.2 Hz, 1H), 4.66 (t, *J* = 4.2 Hz, 1H), 6.68 (s, 1H), 6.75 (d, *J* = 8.7 Hz, 2H), 7.27–7.32 (m, 1H), 7.46 (d, *J* = 9.3 Hz, 1H), 7.57 (d, *J* = 2.2 Hz, 1H), 7.73 (d, *J* = 8.7 Hz, 2H).

2.1.24. 6-(2-(2-Hydroxy-ethoxy)-ethoxy)-4'-methylaminoflavone (16b)

The same reaction as described above to prepare **13** was used, and 41 mg of **16b** was obtained from **14b** in a yield of 37.9%. ¹H NMR (CDCl₃) δ: 3.49 (s, 3H), 3.69 (t, *J* = 3.6 Hz, 2H), 3.77–3.79 (m, 2H), 3.91 (t, *J* = 4.8 Hz, 2H), 4.27 (t, *J* = 4.0 Hz, 2H), 6.65 (s, 1H), 6.68–6.69 (m, 2H), 7.29–7.32 (m, 1H), 7.47 (d, *J* = 9.0 Hz, 1H), 7.65 (d, *J* = 3.0 Hz, 1H), 7.78 (d, *J* = 9.0 Hz, 2H). EI-MS *m/z* 355 (M⁺).

2.1.25. 6-(2-(2-(2-Hydroxy-ethoxy)-ethoxy)ethoxy)-4'-methylaminoflavone (16c)

The same reaction as described above to prepare **13** was used, and 145 mg of **16c** was obtained from **14c** in a yield of 64.8%. ¹H NMR (CDCl₃) δ: 2.92 (d, *J* = 3.0 Hz, 3H), 3.63 (t, *J* = 5.4 Hz, 2H), 3.72–3.76 (m, 6H), 3.91 (t, *J* = 5.1 Hz, 2H), 4.25 (t, *J* = 4.8 Hz, 3H), 6.65 (s, 1H), 6.68 (s, 2H), 7.28–7.32 (m, 1H), 7.46 (d, *J* = 9.3 Hz, 1H), 7.59 (d, *J* = 2.2 Hz, 1H), 7.77 (d, *J* = 8.7 Hz, 2H).

2.1.26. 6-(2-(2-Fluoro-ethoxy)-ethoxy)-4'-methylaminoflavone (17b)

The same reaction as described above to prepare **8** was used, and 9 mg of **17b** was obtained from **16b** in a yield of 21.9%. ¹H NMR (CDCl₃) δ: 2.93 (d, *J* = 5.1 Hz, 3H), 3.79 (t, *J* = 4.2 Hz, 1H), 3.85–3.95 (m, 3H), 4.26 (t, *J* = 4.8 Hz, 3H), 4.53 (t, *J* = 4.2 Hz, 1H), 4.70 (t, *J* = 4.5 Hz, 1H), 6.65 (s, 1H), 6.68 (s, 2H), 7.28–7.32 (m, 1H), 7.47 (d, *J* = 9.0 Hz, 1H), 7.59 (d, *J* = 3.0 Hz, 1H), 7.78 (d, *J* = 9.0 Hz, 2H). EI-MS *m/z* 357 (M⁺).

2.1.27. 6-(2-(2-(2-Fluoro-ethoxy)-ethoxy)ethoxy)-4'-methylaminoflavone (17c)

The same reaction as described above to prepare **8** was used, and 20 mg of **17c** was obtained from **16c** in a yield of 13.8%. ¹H NMR (CDCl₃) δ: 2.92 (d, *J* = 4.8 Hz, 3H), 3.69–3.76 (m, 5H), 3.82 (t, *J* = 4.5 Hz, 1H), 3.91 (t, *J* = 4.8 Hz, 2H), 4.25 (t, *J* = 4.2 Hz, 3H), 4.50 (t, *J* = 4.2 Hz, 1H), 4.66 (t, *J* = 4.5 Hz, 1H), 6.65 (s, 1H), 6.68 (s, 2H), 7.28–7.31 (m, 1H), 7.46 (d, *J* = 9.3 Hz, 1H), 7.59 (d, *J* = 3.0 Hz, 1H), 7.77 (d, *J* = 8.7 Hz, 2H). EI-MS *m/z* 401 (M⁺).

2.1.28. 4-Nitrobenzoic acid 2-acetyl-4-fluorophenyl ester (18)

The same reaction as described above to prepare **1** was used, and 2.5 g of **18** was obtained from 2-hydroxy-5-fluoroacetophenone and 4-nitrobenzoyl chloride in a yield of 85.6%. ¹H NMR (300 MHz, CDCl₃) δ: 2.56 (s, 3H), 7.23–7.34 (m, 2H), 7.56–7.60 (m, 1H), 8.37 (s, 4H).

2.1.29. 1-(5-Fluoro-2-hydroxyphenyl)-3-(4-nitrophenyl)propane-1,3-dione (19)

The same reaction as described above to prepare **2** was used, and 2.5 g of **19** was obtained from **18** in a yield of 96.3%. ¹H NMR

(300 MHz, CDCl₃) δ: 6.81 (s, 2H), 7.02 (d, *J* = 9.0 Hz, 1H), 7.45 (d, *J* = 9.0 Hz, 1H), 7.68 (s, 1H), 8.11 (d, *J* = 8.7 Hz, 2H), 8.36 (d, *J* = 8.7 Hz, 2H), 11.7 (s, 1H).

2.1.30. 6-Fluoro-4'-nitroflavone (20)

The same reaction as described above to prepare **3** was used, and 2.0 g of **20** was obtained from **19** in a yield of 85.3%. EI-MS *m/z* 285 (M⁺).

2.1.31. 6-Fluoro-4'-aminoflavone (21)

The same reaction as described above to prepare **4** was used, and 944 mg of **21** was obtained from **20** in a yield of 67.4%. ¹H NMR (300 MHz, CDCl₃) δ: 4.13 (s, broad, 2H), 6.74 (s, 1H), 6.76 (d, *J* = 9.0 Hz, 2H), 7.35–7.42 (m, 1H), 7.51–7.56 (m, 1H), 7.75 (d, *J* = 8.7 Hz, 2H), 7.82–7.85 (m, 1H).

2.1.32. 6-Fluoro-4'-methylaminoflavone (22)

To a mixture of **21** (300 mg, 1.2 mmol) and paraformaldehyde (179 mg, 5.9 mmol) in MeOH (15 mL) was added a solution of NaOMe (0.34 mL, 28 wt % in MeOH) dropwise at 0 °C. The mixture was stirred under reflux for 1 h. After addition of NaBH₄ (246 mg, 6.5 mmol), the solution was heated under reflux for 45 min. To the cold mixture, 1 M NaOH was added followed by extraction with CHCl₃. The organic phase was dried over Na₂SO₄ and filtered. The solvent was removed, and the residue was purified by silica gel chromatography (hexane/ethyl acetate = 5:3) to give 314 mg of **22** (99.2%). ¹H NMR (300 MHz, CDCl₃) δ: 2.91 (s, 3H), 4.37 (s, broad, 1H), 6.63 (s, 1H), 6.66 (s, 2H), 7.32–7.39 (m, 1H), 7.49–7.53 (m, 1H), 7.74 (d, *J* = 8.7 Hz, 2H), 7.82–7.85 (m, 1H).

2.1.33. 6-Fluoro-4'-dimethylaminoflavone (23)

The same reaction as described above to prepare **5** was used, and 203 mg of **23** was obtained from **21** in a yield of 61.0%. ¹H NMR (300 MHz, CDCl₃) δ: 3.08 (s, 6H), 6.69 (s, 1H), 6.76 (d, *J* = 9.3 Hz, 2H), 7.35–7.41 (m, 1H), 7.51–7.56 (m, 1H), 7.81 (d, *J* = 9.0 Hz, 2H), 7.83–7.86 (m, 1H).

2.1.34. 6-(2-Tosyloxyethoxy)-4'-dimethylaminoflavone (24a)

To a solution of **8a** (136 mg, 0.28 mmol) in pyridine (4 mL) was added tosyl chloride (122 mg, 0.65 mmol) in an ice bath. The reaction mixture was stirred for 32 h at room temperature following the reaction in an ice bath for 1 h. The organic phase was dried over Na₂SO₄ and filtered. The solvent was removed, and the residue was purified by silica gel chromatography (chloroform/MeOH = 20:1) to give 50 mg of **24a** (36.8%). ¹H NMR (300 MHz, CDCl₃) δ: 2.45 (s, 3H), 3.07 (s, 6H), 4.23 (t, 2H, *J* = 4.5 Hz), 4.41 (t, *J* = 5.1 Hz, 2H), 6.68 (s, 1H), 6.75 (d, *J* = 9.0 Hz, 2H), 7.12–7.18 (m, 1H), 7.35 (d, *J* = 8.1 Hz, 2H), 7.43–7.56 (m, 2H), 7.82 (t, *J* = 9.0 Hz, 4H). EI-MS: *m/z* 479 [M⁺].

2.1.35. 6-(2-(2-Tosyloxyethoxy)ethoxy)-4'-dimethylaminoflavone (24b)

The same reaction as described above to prepare **24a** was used, and 111 mg of **24b** was obtained from **8b** in a yield of 34.1%. ¹H NMR (300 MHz, CDCl₃) δ: 2.41 (s, 3H), 3.08 (s, 6H), 3.76–3.85 (m, 4H), 4.12 (t, *J* = 5.1 Hz, 2H), 4.22 (t, *J* = 5.1 Hz, 2H), 6.70 (s, 1H), 6.76 (d, *J* = 9.0 Hz, 2H), 7.25–7.33 (m, 3H), 7.47 (d, *J* = 9.0 Hz, 1H), 7.55 (d, *J* = 3.0 Hz, 1H), 7.79–7.83 (m, 4H). EI-MS *m/z* 523 (M⁺).

2.1.36. 6-(2-(2-(2-Tosyloxyethoxy)ethoxy)ethoxy)-4'-dimethylaminoflavone (24c)

The same reaction as described above to prepare **24a** was used, and 35 mg of **24c** was obtained from **8c** in a yield of 39.9%. ¹H NMR (300 MHz, CDCl₃) δ: 2.43 (s, 3H), 3.08 (s, 6H), 3.62–3.73 (m, 6H), 3.87 (t, *J* = 4.8 Hz, 2H), 4.16–4.21 (m, 4H), 6.70 (s, 1H), 6.76 (d, *J* = 9.0 Hz, 2H), 7.28–7.33 (m, 3H), 7.47 (d, *J* = 9.0 Hz, 1H), 7.60 (d, *J* = 2.2 Hz, 1H), 7.79–7.83 (m, 4H). EI-MS *m/z* 567 (M⁺).

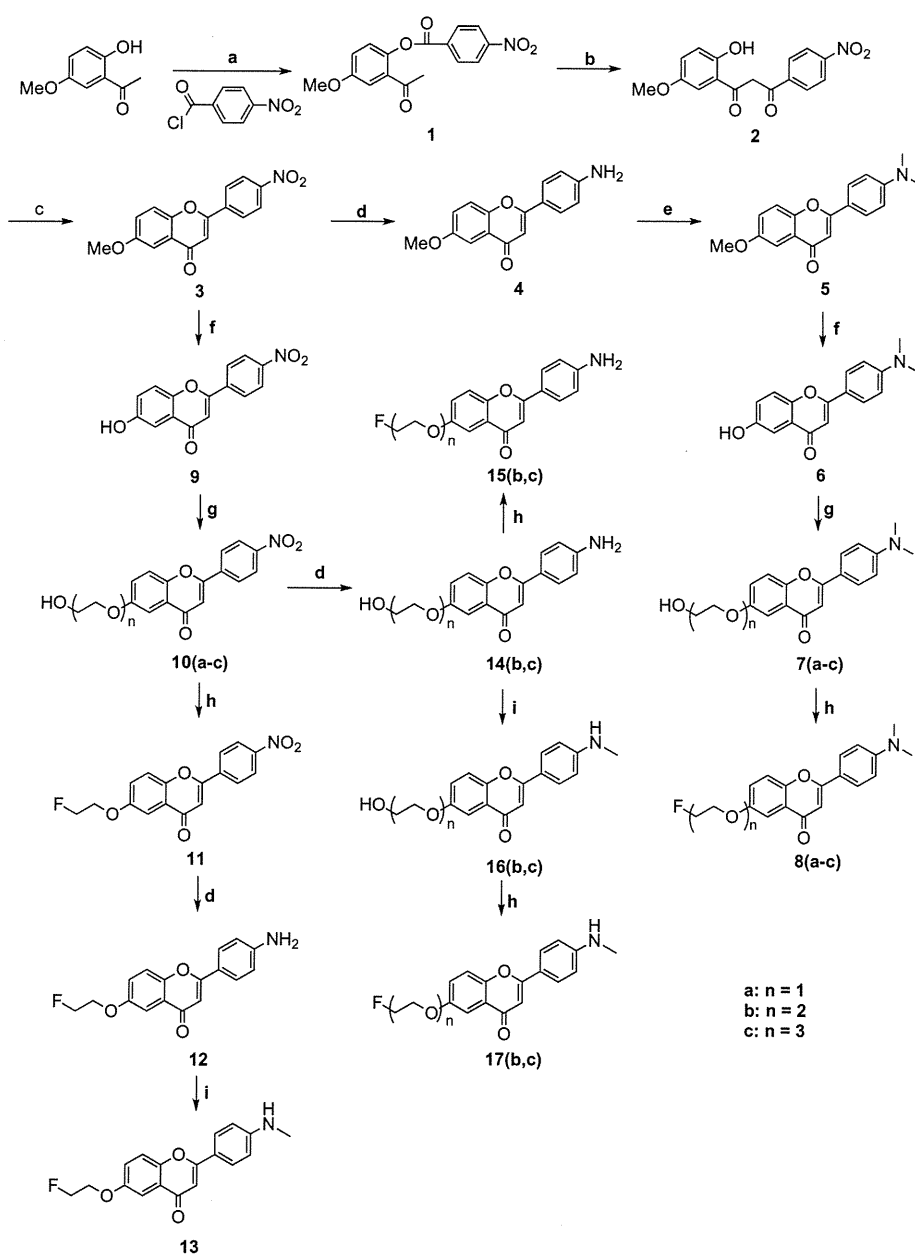
2.2. Radiolabeling

[¹⁸F]Fluoride produced by an ultracompact cyclotron (CYPRIS model 325R; Sumitomo Heavy Industry Ltd) via an ¹⁸O(p,n)¹⁸F reaction was adsorbed to a strong-base anion exchange resin (Bio-Rad), and was eluted with 500 μL of K₂CO₃ solution (33 mM) into 1 mL of acetonitrile containing Kryptofix 222 (K222) (20 mg). The solvent was removed azeotropically with anhydrous acetonitrile at 120 °C under a nitrogen stream. A solution of tosylate precursor **24(a–c)** (0.2 mg) in 400 μL of DMSO was added to the reaction vessel containing [¹⁸F]Fluoride. The mixture was heated at 160 °C for 5 min. The reaction mixture was purified by the reversed phase HPLC system (a Shimadzu LC-6A isocratic pump, a Shimadzu SPD-6A UV detector and an Aloka NDW-351D

scintillation detector) on a YMC Hydrosphere C18 column (20 × 150 mm) with acetonitrile/water (70:30) at a flow rate of 9.0 mL/min to obtain [¹⁸F]**8(a–c)**. The radiochemical purity and specific activity were determined by analytical HPLC on a YMC Pack Pro C18 column (4.6 × 150 mm, acetonitrile/water (60:40), 1.0 mL/min).

2.3. Binding assays using the aggregated Aβ peptide in solution

A solid form of Aβ(1–42) was purchased from Peptide Institute (Osaka, Japan). Aggregation of peptides was carried out by gently dissolving the peptide (0.25 mg/mL) in a buffer solution (pH 7.4) containing 10 mM sodium phosphate and 1 mM EDTA. The solutions were incubated at 37 °C for 42 h with gentle and constant



Scheme 1. Reagents: (a) pyridine; (b) KOH, pyridine; (c) H₂SO₄, AcOH; (d) EtOH, SnCl₂; (e) (CH₂O)_n, NaCNBH₃, AcOH; (f) CH₂Cl₂, BBr₃; (g) Cl(CH₂)_nH (n = 1–3) K₂CO₃, DMF; (h) DAST, DME; (i) DMSO, CH₃I, K₂CO₃.

shaking. Binding experiments were carried out as described previously.¹⁴ [¹²⁵I]DMFV ([¹²⁵I]6-iodo-4'-dimethylaminoflavone) with 81.4 TBq/mmol specific activity and greater than 95% radiochemical purity was prepared using the standard iododestannylation reaction.¹⁴ A mixture containing 50 μ L of test compounds (0.2 pM–400 μ M in 10% EtOH), 50 μ L of 0.02 nM [¹²⁵I]DMFV, 50 μ L of A β (1–42) aggregates and 850 μ L of 10% EtOH was incubated at room temperature for 3 h. The mixture was then filtered through Whatman GF/B filters using a Brandel M-24 cell harvester, and the radioactivity on the filters containing the bound [¹²⁵I] ligand was measured in a gamma counter (Aloka, ARC-380). Values for the half-maximal inhibitory concentration (IC₅₀) were determined from displacement curves of three independent experiments using GraphPad Prism 4.0, and those for the inhibition constant (K_i) were calculated using the Cheng-Prusoff equation:¹⁸ $K_i = IC_{50}/(1 + [L]/K_d)$, where [L] is the concentration of [¹²⁵I]DMFV used in the assay, and K_d is the dissociation constant of DMFV (12.3 nM).¹⁴

2.4. Staining of amyloid plaques in transgenic mouse brain sections

Animal studies were conducted in accordance with institutional guidelines and approved by the Kyoto University Animal Care Committee. Tg2576 transgenic mice (female, 20-month-old) were used as an Alzheimer's model. While under isoflurane anesthesia, the mice were sacrificed by decapitation, and the brains were immediately removed and frozen in powdered dry ice. The frozen blocks were sliced into serial sections 10 μ m thick using a cryostat (Leica Instruments, CM1900). Each slide was incubated with a 50% ethanol solution (100 μ M) of compound **8a**, **8b**, or **8c**, which have the characteristics to emit fluorescence. The sections were washed in 50% ethanol for 3 min two times, and examined using a microscope (Nikon, Eclipse 80i) equipped with a B-2A filter set (excitation, 450–490 nm; dichronic mirror,

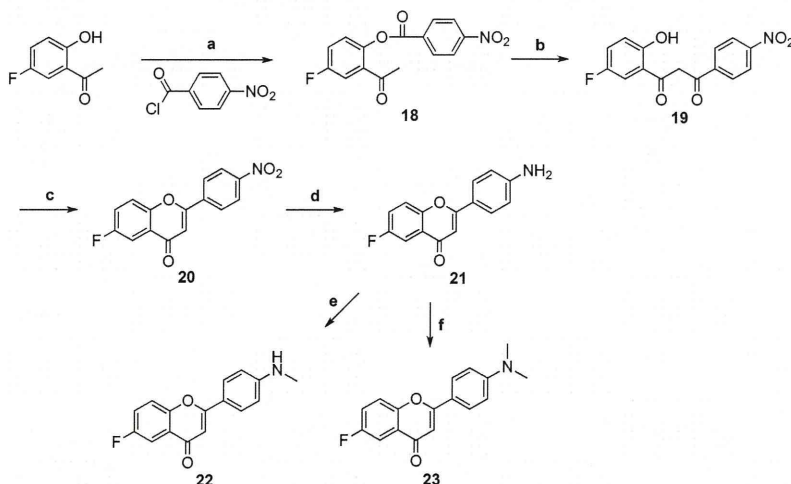
505 nm; longpass filter, 520 nm). Thereafter, the serial sections were also immunostained with DAB as a chromogen using monoclonal antibodies against β -amyloid (Amyloid β -Protein Immunohistostain kit, WAKO).

2.5. In vivo biodistribution in normal mice

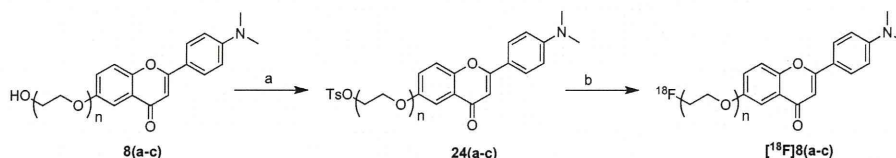
A saline solution (100 μ L) containing ethanol (5 μ L) of radiolabeled agents (18.5 kBq) was injected directly into a tail vein of ddY mice (5-week-old, 22–25 g). While under isoflurane anesthesia, the mice were sacrificed at various time points postinjection. The organs of interest were removed and weighed, and radioactivity was measured with an automatic gamma counter (Packard Cobra Auto-Gamma Counter 5003).

3. Results and discussion

The target FPEG flavone derivatives were prepared as shown in Scheme 1. The most common method of synthesizing flavones is known as the Baker-Venkatarman transformation.¹⁹ In this process, a hydroxyacetophenone is first converted into a benzoyl ester **1**, and this species is then treated with a base, forming a 1,3-diketone **2**. Treatment of this diketone with acid leads to generation of the desired flavone **3**. In the route for the synthesis of dimethylamino derivatives, the free amino derivative **4** was readily prepared from **3** by reduction with SnCl₂. Compound **5** was converted to **6** by demethylation with BBr₃ in CH₂Cl₂. To prepare compounds with 1–3 ethoxy groups as the PEG linkage, commercially available chlorides were coupled with the OH group of **6** to obtain **7(a–c)**, respectively. The fluorinated flavones, **8(a–c)**, were successfully obtained by reacting **7(a–c)** with DAST in DME or ethylene glycol dimethyl ether. In the route for the synthesis of monomethylated derivatives and the primary amino derivatives, the demethylation of **3** with BBr₃ and the introduction of 1–3 ethoxy groups into **9** gave **10(a–c)**. To prepare



Scheme 2. Reagents: (a) pyridine; (b) KOH, pyridine; (c) H₂SO₄, AcOH; (d) EtOH, SnCl₂; (e) (CH₂O)_n, NaOMe, NaBH₄; (f) (CH₂O)_n, NaCNBH₃, AcOH.



Scheme 3. Reagents: (a) tosyl chloride, pyridine; (b) K₂CO₃, [¹⁸F]F⁻, kryptofix[222], DMSO/acetonitrile.

the FPEG flavone with one ethoxy group ($n = 1$) (**12** and **13**), the fluorination of **10a** with DAST, the reduction of **11** with SnCl_2 and the methylation of **12** were performed. The primary amino derivatives of FPEG flavones ($n = 2$ and 3) (**15b** and **15c**) were synthesized by the fluorination of **14b** and **14c** with DAST following the reduction of the nitro group in **10b** and **10c**. The monomethylated FPEG flavones ($n = 2$ and 3) (**17b** and **17c**) were synthesized by the methylation of **16b** and **16c** following the fluorination of **14b** and **14c** with DAST. We successfully synthesized the flavone derivatives (**21**, **22**, and **23**) with fluorine directly bound to the phenyl group according to a procedure reported previously (Scheme 2). To make the desired ^{18}F -labeled FPEG flavones, ^{18}F **8(a-c)**, the tosylates **24(a-c)** were

employed as the precursors. The free OH groups of **8(a-c)** were converted into tosylates by reacting with TsCl in the presence of pyridine to give **24(a-c)** (Scheme 3). Each of the tosylates, **24(a-c)**, was mixed with ^{18}F fluoride/potassium carbonate and Kryptofix 222 in DMSO and heated at 160°C for 5 min. The crude product was purified by HPLC (radiochemical purity >99%, radiochemical yield 5–13%, decay corrected). The total synthesis time was 70 min, and the specific activity was estimated to be 33.3–55.5 GBq/mmol at the end of synthesis.

In vitro binding experiments to evaluate the affinity of the FPEG flavones for $\text{A}\beta$ aggregates were carried out in solutions with ^{125}I DMFV as the ligand. The affinity of flavone derivatives for $\text{A}\beta$ aggregates varied from 5 to 321 nM (Table 1). The flavone derivatives had affinity for $\text{A}\beta(1-42)$ aggregates in the following order: the dimethylamino derivatives (**8a**, **8b**, **8c**, and **23**) > the monomethylamino derivatives (**13**, **17b**, **17c**, and **22**) > the primary amino derivatives (**12**, **15b**, **15c**, and **21**). The results of the binding experiments are consistent with those of previous reports.^{14,20,21} The K_i values indicated that the affinity for $\text{A}\beta(1-42)$ aggregates was affected by the substituted group at position 4' in the flavone structure, not by the length of the PEG introduced into the flavone backbone. We selected the dimethylamino derivatives (**8a**, **8b**, and **8c**), which showed greater binding affinity than the monomethylamino derivatives and the primary amino derivatives, for additional study.

Three ^{18}F FPEG flavones (^{18}F **8a**, ^{18}F **8b**, and ^{18}F **8c**) were examined for their biodistribution in normal mice (Table 2). All three ligands displayed high uptake from the brain 2.89–4.17%ID/g, at 2 min postinjection, indicating a level sufficient for imaging. In addition, they displayed good clearance from the normal brain with 1.89, 2.00, and 1.31%ID/g at 30 min postinjection for ^{18}F **8a**, ^{18}F **8b**, and ^{18}F **8c**, respectively. These values were equal to 45.3%, 56.5%, and 45.3% of the initial uptake peak for ^{18}F **8a**, ^{18}F **8b**, and ^{18}F **8c**, respectively. A rapid initial uptake in normal brain coupled with a fast washout are highly desirable properties for β -amyloid-imaging probes, as they lead to a high signal to background ratio. ^{18}F **8(a-c)** showed the bone uptake (3.74–6.21%ID/g) at 60 min postinjection, suggesting there may be in vivo defluorination. However, the free fluorine was not taken up by brain tissue; therefore, the interference from this free fluoride is expected to be relatively low for brain imaging.²²

To confirm the affinity of FPEG chalcone derivatives for β -amyloid plaques in the brain, neuropathological fluorescent staining

Table 1
Inhibition constants (K_i , nM) of compounds for the binding of ^{125}I DMFV to $\text{A}\beta(1-42)$ aggregates^a

Compound	K_i (nM)	Compound	K_i (nM)
8a	5.3 ± 0.8	15c	234.0 ± 60.6
8b	14.4 ± 2.5	17b	54.5 ± 10.3
8c	19.3 ± 4.0	17c	45.1 ± 5.8
12	234.3 ± 63.5	21	260.5 ± 43.3
13	99.0 ± 11.8	22	110.0 ± 47.4
15b	321.1 ± 74.4	23	73.9 ± 5.3

^a Values are the mean \pm standard error of the mean for 4–9 experiments.

Table 2
Biodistribution of ^{18}F -labeled flavones in normal mice^a

Organ	2 min	10 min	30 min	60 min
^{18}F 8a				
Blood	2.80 ± 0.41	2.71 ± 0.13	2.53 ± 0.17	3.25 ± 0.31
Brain	4.17 ± 0.77	3.62 ± 0.21	1.89 ± 0.13	2.19 ± 0.18
Bone	2.02 ± 0.53	2.83 ± 0.23	4.51 ± 0.55	6.21 ± 0.84
^{18}F 8b				
Blood	2.09 ± 0.35	2.30 ± 0.07	2.50 ± 0.21	2.94 ± 0.27
Brain	3.54 ± 0.54	2.75 ± 0.21	2.00 ± 0.20	2.13 ± 0.10
Bone	1.13 ± 0.22	1.65 ± 0.10	2.42 ± 0.38	3.74 ± 0.30
^{18}F 8c				
Blood	2.35 ± 0.54	1.50 ± 0.26	1.40 ± 0.04	1.88 ± 0.08
Brain	2.89 ± 0.74	2.23 ± 0.36	1.31 ± 0.14	1.37 ± 0.11
Bone	1.53 ± 0.52	2.38 ± 0.39	4.06 ± 0.49	5.21 ± 0.98

^a Expressed as % of injected dose per gram. Each value represents the mean \pm SD for 4–5 mice at each interval.

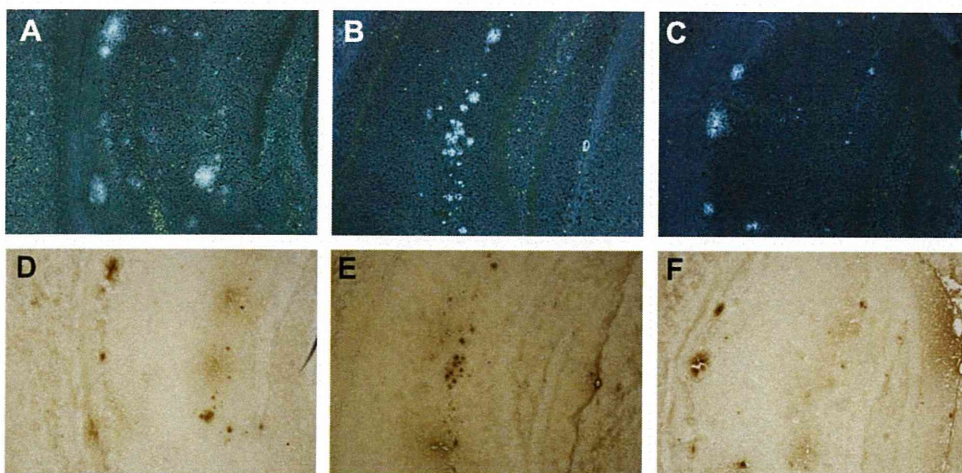


Figure 2. Neuropathological staining of flavone derivatives **8a** (A), **8b** (B), and **8c** (C) in 10- μm brain sections of Tg2576 mice. Immunohistological staining with an antibody against β -amyloid (D, E, and F) in the adjacent sections of A, B, and C, respectively.

with **8a**, **8b**, and **8c** was carried out using the Alzheimer's model (Fig. 2A–C). Many fluorescence spots were observed in the brain sections of Tg2576 transgenic (female, 20-month-old) mice, while no spots were observed in the brain sections of wild-type (female, 22-month-old) mice (data not shown). The fluorescent labeling pattern was consistent with that obtained by immunohistochemical labeling with an antibody specific for A β (Fig. 2D–F), indicating that FPEG flavones show specific binding to β -amyloid plaques in the mouse brain.

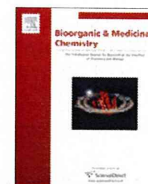
In conclusion, we successfully designed and synthesized novel ^{18}F labeled flavones with the FPEG strategy for PET imaging of β -amyloid in the brain. The affinity of the derivatives for A β aggregates varied from 5 to 321 nM. When in vitro plaque labeling was carried out using sections of brain from Tg2576 mice, FPEG flavones intensely stained β -amyloid plaques. In addition, they displayed good uptake into and a rapid washout from the brain after injection in normal mice. The combination of high binding affinity for β -amyloid plaques, high brain uptake, and good clearance in mice of the FPEG-flavone derivatives may provide a series of promising in vivo amyloid imaging agents for PET.

Acknowledgments

This study was supported by the Industrial Technology Research Grant Program from the New Energy and Industrial Technology Development Organization (NEDO) of Japan, and the Program for Promotion of Fundamental Studies in Health Sciences of the National Institute of Biomedical Innovation (NIBIO).

References and notes

- Hardy, J. A.; Higgins, G. A. *Science* **1992**, *256*, 184.
- Selkoe, D. J. *Physiol. Rev.* **2001**, *81*, 741.
- Selkoe, D. J. *Nat. Biotechnol.* **2000**, *18*, 823.
- Mathis, C. A.; Wang, Y.; Klunk, W. E. *Curr. Pharm. Des.* **2004**, *10*, 1469.
- Nordberg, A. *Lancet Neurol.* **2004**, *3*, 519.
- Ono, M.; Wilson, A.; Nobrega, J.; Westaway, D.; Verhoeff, P.; Zhuang, Z. P.; Kung, M. P.; Kung, H. F. *Nucl. Med. Biol.* **2003**, *30*, 565.
- Verhoeff, N. P.; Wilson, A. A.; Takeshita, S.; Trop, L.; Hussey, D.; Singh, K.; Kung, H. F.; Kung, M. P.; Houle, S. *Am. J. Geriatr. Psychiat.* **2004**, *12*, 584.
- Mathis, C. A.; Wang, Y.; Holt, D. P.; Huang, G. F.; Debnath, M. L.; Klunk, W. E. *J. Med. Chem.* **2003**, *46*, 2740.
- Klunk, W. E.; Engler, H.; Nordberg, A.; Wang, Y.; Blomqvist, G.; Holt, D. P.; Bergstrom, M.; Savitcheva, I.; Huang, G. F.; Estrada, S.; Ausen, B.; Debnath, M. L.; Barletta, J.; Price, J. C.; Sandell, J.; Lopresti, B. J.; Wall, A.; Koivisto, P.; Antoni, G.; Mathis, C. A.; Langstrom, B. *Ann. Neurol.* **2004**, *55*, 306.
- Kudo, Y.; Okamura, N.; Furumoto, S.; Tashiro, M.; Furukawa, K.; Maruyama, M.; Itoh, M.; Iwata, R.; Yanai, K.; Arai, H. *J. Nucl. Med.* **2007**, *48*, 553.
- Agdeppa, E. D.; Kepe, V.; Liu, J.; Flores-Torres, S.; Satyamurthy, N.; Petric, A.; Cole, G. M.; Small, G. W.; Huang, S. C.; Barrio, J. R. *J. Neurosci.* **2001**, *21*, RC189.
- Shoghi-Jadid, K.; Small, G. W.; Agdeppa, E. D.; Kepe, V.; Ercoi, L. M.; Siddarth, P.; Read, S.; Satyamurthy, N.; Petric, A.; Huang, S. C.; Barrio, J. R. *Am. J. Geriatr. Psychiat.* **2002**, *10*, 24.
- Rowe, C. C.; Ackerman, U.; Browne, W.; Mulligan, R.; Pike, K. L.; O'Keefe, G.; Tochon-Danguy, H.; Chan, G.; Berlangieri, S. U.; Jones, G.; Dickinson-Rowe, K. L.; Kung, H. P.; Zhang, W.; Kung, M. P.; Skovronsky, D.; Dyrks, T.; Holl, G.; Krause, S.; Friebe, M.; Lehman, L.; Lindemann, S.; Dinkelborg, L. M.; Masters, C. L.; Villemagne, V. L. *Lancet Neurol.* **2008**, *7*, 129.
- Ono, M.; Yoshida, N.; Ishibashi, K.; Haratake, M.; Arano, Y.; Mori, H.; Nakayama, M. *J. Med. Chem.* **2005**, *48*, 7253.
- Stephenson, K. A.; Chandra, R.; Zhuang, Z. P.; Hou, C.; Oya, S.; Kung, M. P.; Kung, H. F. *Bioconjugate Chem.* **2007**, *18*, 238.
- Ono, M.; Kung, M. P.; Hou, C.; Kung, H. F. *Nucl. Med. Biol.* **2002**, *29*, 633.
- Zhuang, Z. P.; Kung, M. P.; Wilson, A.; Lee, C. W.; Plossl, K.; Hou, C.; Holtzman, D. M.; Kung, H. F. *J. Med. Chem.* **2003**, *46*, 237.
- Cheng, Y.; Prusoff, W. *Biochem. Pharmacol.* **1973**, *1973*, 3099.
- Ares, J. J.; Outt, P. E.; Randall, J. L.; Murray, P. D.; Weisshaar, P. S.; O'Brien, L. M.; Ems, B. L.; Kakodkar, S. V.; Kelm, G. R.; Kershaw, W. C., et al. *J. Med. Chem.* **1995**, *38*, 4937.
- Ono, M.; Haratake, M.; Mori, H.; Nakayama, M. *Bioorg. Med. Chem.* **2007**, *15*, 6802.
- Ono, M.; Hori, M.; Haratake, M.; Tomiyama, T.; Mori, H.; Nakayama, M. *Bioorg. Med. Chem.* **2007**, *15*, 6388.
- Zhang, W.; Oya, S.; Kung, M. P.; Hou, C.; Maier, D. L.; Kung, H. F. *Nucl. Med. Biol.* **2005**, *32*, 799.



Synthesis and biological evaluation of radioiodinated 2,5-diphenyl-1,3,4-oxadiazoles for detecting β -amyloid plaques in the brain

Hiroyuki Watanabe^a, Masahiro Ono^{a,b,*}, Ryoichi Ikeoka^a, Mamoru Haratake^a, Hideo Saji^b, Morio Nakayama^{a,*}

^a Graduate School of Biomedical Sciences, Nagasaki University, 1-14 Bunkyo-machi, Nagasaki 852-8521, Japan

^b Graduate School of Pharmaceutical Sciences, Kyoto University, 46-29 Yoshida Shimoadachi-cho, Sakyo-ku, Kyoto 606-8501, Japan

ARTICLE INFO

Article history:

Received 2 June 2009

Revised 10 July 2009

Accepted 11 July 2009

Available online 17 July 2009

Keywords:

Alzheimer's disease

β -Amyloid plaques

SPECT imaging

ABSTRACT

This paper describes the synthesis and biological evaluation of a new series of 2,5-diphenyl-1,3,4-oxadiazole (1,3,4-DPOD) derivatives for detecting β -amyloid plaques in Alzheimer's brains. The affinity for β -amyloid plaques was assessed by an in vitro binding assay using pre-formed synthetic A β 42 aggregates. The new series of 1,3,4-DPOD derivatives showed affinity for A β 42 aggregates with K_i values ranging from 20 to 349 nM. The 1,3,4-DPOD derivatives clearly stained β -amyloid plaques in an animal model of Alzheimer's disease, reflecting the affinity for A β 42 aggregates in vitro. Compared to 3,5-diphenyl-1,2,4-oxadiazole (1,2,4-DPOD) derivatives, they displayed good penetration of and fast washout from the brain in biodistribution experiments using normal mice. The novel radioiodinated 1,3,4-DPOD derivatives may be useful probes for detecting β -amyloid plaques in the Alzheimer's brain.

© 2009 Elsevier Ltd. All rights reserved.

1. Introduction

Alzheimer's disease (AD) is a progressive neurodegenerative disorder pathologically characterized by the deposition of β -amyloid (A β) peptides as senile plaques in the brain.^{1,2} Since the deposition of A β plaques is an early event in the development of AD, a validated biomarker of A β deposition in the brain would likely prove useful for identifying and following individuals at risk for AD and assist in the evaluation of new anti-amyloid therapies currently under development. Therefore, the quantitative evaluation of A β plaques in the brain with non-invasive techniques such as positron emission tomography (PET) and single photon emission computed tomography (SPECT) could lead to the presymptomatic detection of AD and new anti-amyloid therapies.^{3–5}

In the past few years, several groups have reported potential A β -imaging probes for the detection of A β plaques in vivo. Tracers such as [¹¹C]PIB,^{6,7} [¹¹C]SB-13,^{8,9} [¹⁸F]BAY94-9172,¹⁰ [¹¹C]BF-227,¹¹ [¹⁸F]FDDNP,^{12–14} and [¹²³I]IMPY^{15–18} have been tested clinically and demonstrated utility. [¹²³I]IMPY is the only tracer for SPECT, the other five tracers are A β -imaging probes for PET. Since SPECT is more valuable than PET in terms of routine diagnostic use, the development of more useful A β -imaging agents for SPECT has been a critical issue.

Recently, we successfully designed and synthesized a new series of 3,5-diphenyl-1,2,4-oxadiazole (1,2,4-DPOD) derivatives as SPECT probes for the in vivo imaging of A β plaques in the brain.¹⁹ The 1,2,4-DPOD derivatives are categorized into A β -imaging agents with the three-aromatic-ring linked system.^{20–22} The derivatives displayed excellent affinity for A β aggregates in in vitro binding experiments. The degree to which the DPOD derivatives penetrated the brain was also very encouraging. However, nonspecific binding in vivo reflected by a slow washout from the normal mouse brain makes them unsuitable for the imaging of A β plaques. The less than ideal in vivo biodistribution results in normal mice indicate that there is a critical need to fine-tune the kinetics of brain uptake and washout. Additional structural changes, that is, reducing the lipophilicity, are necessary to improve the in vivo properties of the DPOD derivatives.

In an attempt to further develop novel ligands for the imaging of A β plaques in AD, we designed a series of 2,5-diphenyl-1,3,4-oxadiazole (1,3,4-DPOD) derivatives, which are structural isomers of 1,2,4-DPOD and less lipophilic than 1,2,4-DPOD (Fig. 1). To our

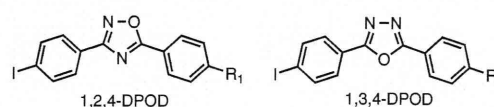


Figure 1. Chemical structure of 1,2,4-DPOD reported previously and 1,3,4-DPOD reported in this paper. R₁ = NH₂, NHCH₃, N(CH₃)₂, OCH₃, OH; R₂ = N(CH₃)₂, OCH₃, OH, OCH₂CH₂OH, (OCH₂CH₂)₂OH, (OCH₂CH₂)₃OH.

* Corresponding authors. Tel.: +81 75 753 4608; fax: +81 75 753 4568 (M.O.); tel./fax: +81 95 819 2441 (M.N.).

E-mail addresses: ono@pharm.kyoto-u.ac.jp (M. Ono), morio@nagasaki-u.ac.jp (M. Nakayama).

knowledge, this is the first time the use of 1,3,4-DPOD derivatives *in vivo* as probes to image A β plaques in the AD brain has been proposed. Described herein is the synthesis of a novel series of 1,3,4-DPOD derivatives and the characterization as A β -imaging probes in comparison with 1,2,4-DPOD derivatives.

2. Results and discussion

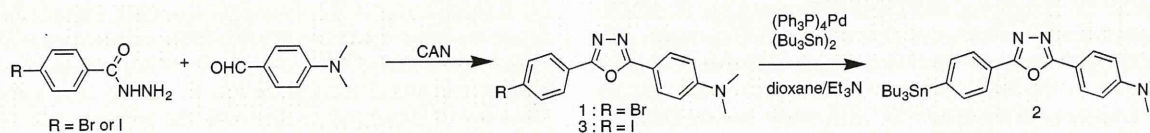
The synthesis of 1,3,4-DPOD derivatives is outlined in Schemes 1 and 2. We used the one-pot synthesis method of producing 2,5-diphenyl-1,3,4-oxadiazoles.²³ The 2,5-diphenyl-1,3,4-oxadiazoles (**3** and **4**) were prepared by 4-iodobenzhydrazide with 4-dimethylaminobenzaldehyde and 4-methoxybenzaldehyde in the presence of ceric ammonium nitrate (CAN). Compound **4** was converted to **6** by demethylation with BBr₃ in CH₂Cl₂ (49% yield). Direct alkylation of **6** with ethylene chlorohydrin, ethylene glycol mono-2-chloroethyl ether, or 2-[2-(2-chloroethoxy)ethoxy]ethanol with potassium carbonate in DMF resulted in **7–9**. The tributyltin derivatives (**2** and **5**) were prepared from corresponding compounds (**1** and **4**) using a halogen to tributyltin exchange reaction catalyzed by Pd(0) for yields of 8.2% and 6.5%, respectively. The tributyltin derivatives were used as the starting materials for radioiodination in the preparation of [¹²⁵I]**3** and [¹²⁵I]**4**. Novel radioiodinated 1,3,4-DPOD derivatives were obtained by an iododestannylation reaction using hydrogen peroxide as the oxidant which produced the desired radioiodinated ligands (Scheme 3). It was anticipated that the no-carrier-added preparation would result in a final product bearing a theoretical specific activity similar to that of ¹²⁵I (2200 Ci/mmol). The radiochemical identity of the radioiodinated ligands was verified by co-injection with non-radioiodinated compounds from their HPLC profiles. [¹²⁵I]**3** and [¹²⁵I]**4** were each obtained in a radiochemical yield of >45% with a radiochemical purity of >95% after purification by HPLC.

The affinity of 1,3,4-DPOD derivatives (**3**, **4**, **6–9**) was evaluated based on inhibition of the binding of [¹²⁵I]IMPY to A β 42 aggregates. As shown in Table 1, all 1,3,4-DPOD derivatives showed inhibitory activity toward A β aggregates. The affinity of 1,3,4-DPOD derivatives for A β aggregates varied from 20 to 349 nM. Compound **3** with the dimethylamino group and **4** with the methoxy group showed high binding affinity with a K_i of 20 and 46 nM, respec-

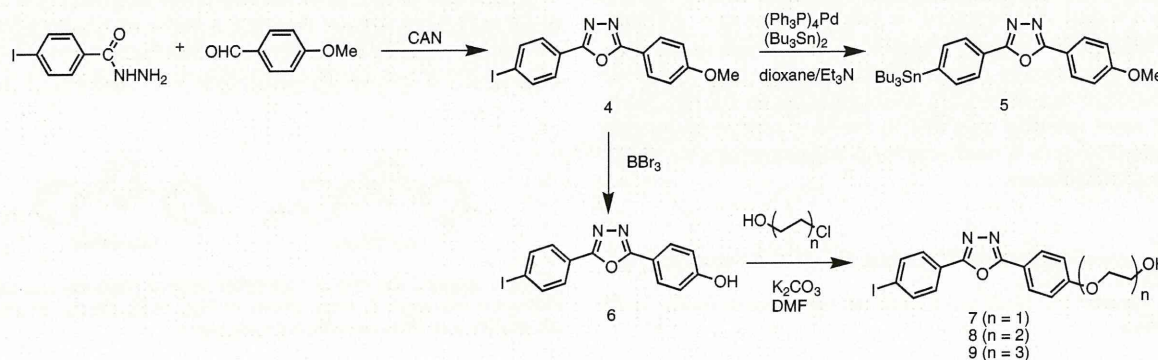
tively, while no marked affinity was observed for **6–9**. Compound **3** displayed almost equal affinity for A β aggregates as the 1,2,4-DPOD derivative with the dimethylamino group (4-(3-(4-iodophenyl)-1,2,4-oxadiazole-5-yl)-*N,N*-dimethylamine; 1,2,4-DPOD-DM, K_i = 15 nM).¹⁹

To confirm the affinity of 1,3,4-DPOD derivatives for A β plaques in the brain, fluorescent staining of sections of mouse brain from an animal model of AD was carried out with compound **3** (Fig. 2). Many fluorescence spots were observed in the brain sections of Tg2576 transgenic mice (female, 28-month-old) (Fig. 2A), while no spots were observed in the brain sections of wild-type mice (female, 28-month-old) (Fig. 2B). The fluorescent labeling pattern was consistent with that observed with thioflavin S (Fig. 2C). These results suggested that **3** shows specific binding to A β plaques in the mouse brain. In the fluorescent staining of Tg2576 mouse brain sections, **4** also showed specific binding to A β plaques in the brain (data not shown).

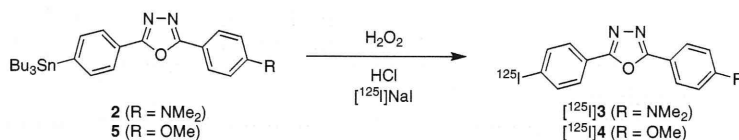
Next, [¹²⁵I]**3** and [¹²⁵I]**4** were evaluated for their *in vivo* biodistribution in normal mice. A biodistribution study provides critical information on brain penetration. Generally, a freely diffusible compound with an optimal log *P* value of 2–3 will have an initial brain uptake of 2–3% dose/whole brain at 2 min after *iv* injection. [¹²⁵I]**3** and [¹²⁵I]**4** examined in this study displayed optimal lipophilicity as reflected by log *P* values of 2.43 and 2.58, respectively (Table 2). As expected, these ligands displayed good brain uptake ranging from 3.8% to 5.9% ID/g brain at 2–10 min postinjection, indicating a level sufficient for brain imaging probes (Table 3). In addition, they displayed good clearance from the normal brain with 1.8% and 0.36% ID/g at 60 min postinjection for [¹²⁵I]**3** and [¹²⁵I]**4**, respectively. These values were equal to a peak in brain uptake of 30% and 9.6%, respectively. Additionally, all of the other organs or tissues displayed a good initial uptake and a relatively fast washout with time. To directly compare the brain uptake and washout of [¹²⁵I]1,2,4-DPOD and [¹²⁵I]1,3,4-DPOD, a combined plot is presented in Figure 3. It is apparent that [¹²⁵I]1,2,4-DPOD showed a lower initial uptake with a longer retention, while [¹²⁵I]1,3,4-DPOD displayed a higher initial uptake but with a faster washout from the brain. At 2 or 10 min after *iv* injection, the uptake of [¹²⁵I]1,3,4-DPOD reached a maximum after which the activity in the normal brain was washed out. It is important to note that



Scheme 1.



Scheme 2.



Scheme 3.

Table 1

Inhibition constants (K_i) for binding of 1,3,4-DPOD derivatives determined using [¹²⁵I]IMPY as the ligand in Aβ₄₂ aggregates

Compound	K_i^a (nM)
3	20.1 ± 2.5
4	46.1 ± 12.6
6	229.6 ± 47.3
7	282.2 ± 61.4
8	348.6 ± 51.7
9	257.7 ± 34.8

^a Values are the mean ± standard error for the mean for 4–6 independent experiments.

Table 2

Partition coefficients for 1,2,4-DPOD and 1,3,4-DPOD derivatives

Compound	Log P^a
3	2.43 ± 0.07
4	2.58 ± 0.06
1,2,4-DPOD-DM	3.22 ± 0.01
1,2,4-DPOD-OMe	3.37 ± 0.04

^a Octanol/buffer (0.1 M phosphate-buffered saline, pH 7.4) partition coefficients. Each value represents the mean ± SD for 2–3 experiments.

the ideal Aβ-imaging agent should have good brain penetration to deliver the intended dose into the brain, while maintaining a fast washout from normal tissues. Because the normal brain has no Aβ plaques to trap the agent, the washout from the brain should also be fast. Once the high affinity ligand is delivered into the regions containing the Aβ plaques, imaging agents such as [¹²⁵I]3 and [¹²⁵I]4 are expected to be trapped in this region longer due to its high binding affinity. The differences between the kinetics in normal and Aβ plaque-containing regions will result in a higher signal to noise ratio (target to non-target ratio) in the AD brain. Based on the data presented for [¹²⁵I]1,3,4-DPOD, it is predicted that the brain trapping of [¹²⁵I]1,3,4-DPOD in Aβ-containing regions will be much better than that of [¹²⁵I]1,2,4-DPOD. The log P values of 1,3,4-DPOD derivatives (log P = 2.43 and 2.58 for 3 and 4, respectively) were lower than those of 1,2,4-DPOD derivatives (log P = 3.22 and 3.37 for 1,2,4-DPOD-DM and 1,2,4-DPOD-OMe, respectively). Although many factors such as molecular size, ionic charge, and lipophilicity affect the uptake of a compound into the brain, the difference in lipophilicity may be one reason for the difference in brain uptake and washout between 1,3,4-DPOD and 1,2,4-DPOD. Further structural modifications, that is, decreasing the lipophilicity by introducing the hydrophilic group, should improve the in vivo properties of 1,3,4-DPOD derivatives.

3. Conclusion

In conclusion, we successfully designed and synthesized a new series of 1,3,4-DPOD derivatives as probes for the in vivo imaging of Aβ plaques in the brain. In in vitro binding experiments, these

Table 3

Biodistribution of radioactivity after injection of [¹²⁵I]1,3,4-DPOD derivatives in normal mice^a

Tissue	Time after injection (min)			
	2	10	30	60
[¹²⁵ I]3				
Blood	3.28 (0.46)	3.51 (0.29)	2.53 (0.28)	2.21 (0.41)
Liver	15.87 (3.49)	19.12 (2.43)	12.64 (2.44)	10.01 (1.64)
Kidney	9.14 (1.60)	7.80 (0.64)	5.71 (1.35)	3.81 (0.64)
Intestine	2.28 (0.55)	11.34 (1.61)	12.58 (2.35)	16.22 (2.51)
Spleen	3.56 (0.96)	4.10 (0.40)	2.63 (0.54)	2.05 (0.41)
Pancreas	5.32 (0.98)	4.39 (2.17)	2.50 (0.56)	2.14 (0.90)
Heart	3.99 (3.10)	3.55 (1.86)	2.03 (0.30)	1.54 (0.31)
Stomach ^b	1.40 (0.10)	4.73 (1.86)	4.79 (1.12)	5.50 (0.51)
Brain	2.98 (0.53)	5.93 (0.76)	3.16 (0.69)	1.78 (0.41)
[¹²⁵ I]4				
Blood	1.84 (0.30)	1.60 (0.30)	1.26 (0.26)	0.80 (0.20)
Liver	9.60 (1.73)	12.60 (1.14)	8.07 (1.66)	4.65 (1.34)
Kidney	7.14 (1.46)	4.85 (0.48)	4.36 (1.12)	2.48 (0.37)
Intestine	2.07 (0.36)	4.49 (0.60)	10.06 (1.81)	19.85 (4.71)
Spleen	2.44 (0.28)	1.51 (0.26)	0.80 (0.10)	0.60 (0.26)
Pancreas	4.74 (0.63)	1.98 (0.37)	0.96 (0.03)	0.57 (0.14)
Heart	4.80 (1.33)	1.73 (0.27)	0.92 (0.25)	0.43 (0.11)
Stomach ^b	0.71 (0.13)	1.41 (0.91)	3.12 (0.90)	2.90 (1.57)
Brain	3.75 (0.78)	2.74 (0.37)	1.04 (0.14)	0.36 (0.13)

^a Expressed as % injection dose per gram. Each value represents the mean (SD) for 4–6 animals.

^b Expressed as % injected dose per organ.

1,3,4-DPOD derivatives showed affinity for Aβ₄₂ aggregates. The 1,3,4-DPOD derivatives clearly stained Aβ plaques in an animal model of AD, reflecting their affinity for Aβ aggregates in vitro. Compared to 1,2,4-DPOD, they displayed good penetration of and a fast washout from the brain in biodistribution experiments using

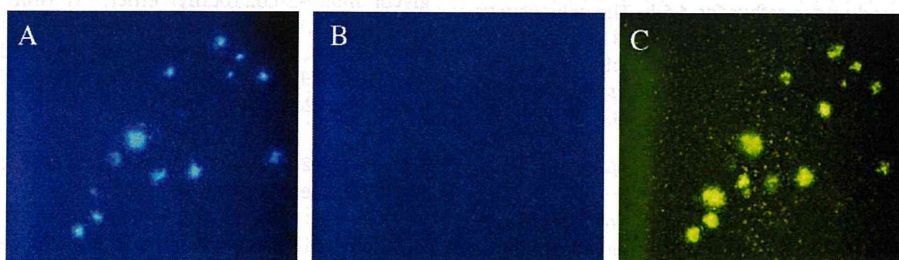


Figure 2. Neuropathological staining of compound 3 on 10-µm AD model mouse sections (A) and wild-type mouse sections (B). Labeled plaques were confirmed by staining of the adjacent sections with thioflavin S (C).

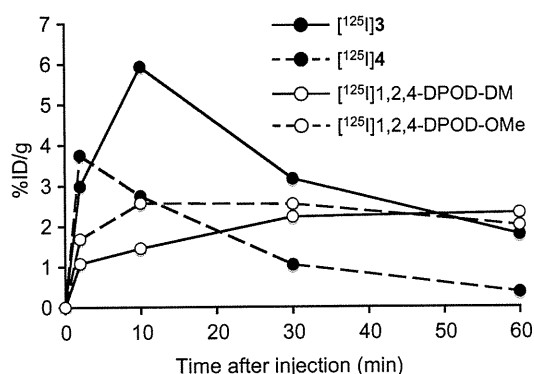


Figure 3. Comparison of brain uptake of [¹²⁵I]3, [¹²⁵I]4, [¹²⁵I]1,2,4-DPOD-DM and [¹²⁵I]1,2,4-DPOD-OMe in normal mice. The kinetics of the uptake of [¹²⁵I]3 and [¹²⁵I]4 may provide a better pattern for the localization of Aβ plaques in the brain.

normal mice. Taken together, the present results suggested that the novel radiiodinated 1,3,4-DPOD derivatives may be useful probes for detecting Aβ plaques in the AD brain.

4. Experimental

4.1. General

All reagents were commercial products and used without further purification unless otherwise indicated. ¹H NMR spectra were obtained on a Varian Gemini 300 spectrometer with TMS as an internal standard. Coupling constants are reported in hertz. Multiplicity is defined by s (singlet), d (doublet), t (triplet), and m (multiplet). ¹³C NMR spectra were obtained on an AL400 JEOL spectrometer with TMS as an internal standard. Mass spectra were obtained on a JEOL IMS-DX.

4.1.1. 4-(5-(4-Bromophenyl)-1,3,4-oxadiazol-2-yl)-N,N-dimethylbenzenamine (1)

To a solution of 4-bromobenzhydrazide (215 mg, 1 mmol) and 4-dimethylaminobenzaldehyde (149 mg, 1 mmol) in dry CH₂Cl₂ (10 mL) was added CAN (548 mg, 1 mmol). The reaction mixture was stirred under reflux for 24 h. Water was added and following extraction with CHCl₃, the organic phase was dried over Na₂SO₄. The solvent was removed and the residue was purified by silica gel chromatography (hexane/ethyl acetate = 4:1) to give 12 mg of **1** (3.5%). ¹H NMR (300 MHz, CDCl₃) δ 3.08 (s, 6H), 6.76 (d, J = 9.0 Hz, 2H), 7.66 (d, J = 8.4 Hz, 2H), 7.98 (dd, J = 5.4, 4.5 Hz, 4H). MS *m/z* 362 (M⁺).

4.1.2. 4-(5-(4-Tributylstannyl)phenyl)-1,3,4-oxadiazol-2-yl)-N,N-dimethylbenzenamine (2)

A mixture of **1** (19 mg, 0.06 mmol), bis(tributyltin) (0.04 mL) and (Ph₃P)₄Pd (3 mg, 0.002 mmol) in a mixed solvent (6 mL, 1:1 dioxane/Et₃N) was stirred under reflux for 4.5 h. The solvent was removed, and the residue was purified by silica gel chromatography (hexane/ethyl acetate = 3:1) to give 2.5 mg of **2** (8.2%). ¹H NMR (300 MHz, CDCl₃) δ 0.87–1.6 (m, 27H), 3.07 (s, 6H), 6.77 (d, J = 9.0 Hz, 2H), 7.61 (d, J = 8.4 Hz, 2H), 8.01 (dd, J = 9.0, 8.1 Hz, 4H).

4.1.3. 4-(5-(Iodophenyl)-1,3,4-oxadiazol-2-yl)-N,N-dimethylbenzenamine (3)

The same reaction as described above to prepare **1** was used, and 14 mg of **3** was obtained in a 1.8% yield from 4-iodobenzhydrazide and 4-dimethylaminobenzaldehyde. ¹H NMR (300 MHz, CDCl₃) δ 3.07 (s, 6H), 6.76 (d, J = 3.0 Hz, 2H), 7.85 (d, J = 12.0 Hz,

4H), 7.97 (d, J = 3.0 Hz, 2H). ¹³C NMR (400 MHz, CDCl₃) δ 40.1, 97.8, 110.7, 111.6, 123.9, 128.0, 128.4, 138.2, 152.5, 162.9, 165.5. HRMS *m/z* C₁₆H₁₄N₃OI found 391.0191/ calcd 391.0182 (M⁺).

4.1.4. 2-(4-Iodophenyl)-5-(4-methoxyphenyl)-1,3,4-oxadiazole (4)

The same reaction as described above to prepare **1** was used, and 40 mg of **4** was obtained in a 8.8% yield from 4-iodobenzhydrazide and 4-methoxybenzaldehyde. ¹H NMR (300 MHz, CDCl₃) δ 3.89 (s, 3H), 7.03 (d, J = 2.9 Hz, 2H), 7.86 (q, J = 7.8 Hz, 4H), 8.03 (d, J = 3.0 Hz, 2H). ¹³C NMR (400 MHz, CDCl₃) δ 55.5, 98.2, 114.6, 116.2, 123.6, 128.1, 128.8, 138.3, 162.5, 163.6, 164.7. HRMS *m/z* C₁₅H₁₁N₂O₂I found 377.9877, calcd 377.9865 (M⁺).

4.1.5. 2-(4-(Tributylstannyl)phenyl)-5-(4-methoxyphenyl)-1,3,4-oxadiazole (5)

The same reaction as described above to prepare **2** was used, and 6 mg of **5** was obtained in a 6.5% yield from **4**. ¹H NMR (300 MHz, CDCl₃) δ 0.87–1.58 (m, 27H), 3.91 (s, 3H), 7.04 (d, J = 3.1 Hz, 2H), 7.63 (d, J = 2.6 Hz, 2H), 8.06 (q, J = 6.6 Hz, 4H).

4.1.6. 4-(5-(4-Iodophenyl)-1,3,4-oxadiazol-2-yl)phenol (6)

BBr₃ (0.6 mL, 1 M solution in CH₂Cl₂) was added to a solution of **4** (36 mg, 0.1 mmol) in CH₂Cl₂ (16 mL) dropwise in an ice bath. The mixture was allowed to warm to room temperature and stirred for 5 days. Water (50 mL) was added while the reaction mixture was cooled in an ice bath. The mixture was extracted with CHCl₃ (30 mL) and the water layer was extracted with ethyl acetate. The organic phase was dried over Na₂SO₄ and filtered. The solvent was removed, and the residue was purified by silica gel chromatography (hexane/ethyl acetate = 2:1) to give 17 mg of **6** (49.0%). ¹H NMR (300 MHz, CDCl₃) δ 6.98–7.06 (m, 2H), 7.86–7.91 (m, 4H), 8.02–8.09 (m, 2H). HRMS *m/z* C₁₄H₉N₂O₂I found 363.9712, calcd 363.9709 (M⁺).

4.1.7. 2-(4-(5-(4-Iodophenyl)-1,3,4-oxadiazol-2-yl)phenoxy)ethanol (7)

A mixture of **6** (22 mg, 0.06 mmol), potassium carbonate (24.5 mg, 0.18 mmol) and ethylene chlorohydrin (4 μL, 0.06 mmol) in anhydrous DMF (3 mL) was stirred under reflux for 6.5 h. After cooling to room temperature, water was added, and the reaction mixture was extracted with CHCl₃. The organic layer was separated, dried over Na₂SO₄ and evaporated. The resulting residue was purified by silica gel chromatography (hexane/ethyl acetate = 2:3) to give 11 mg of **7** (44.6%). ¹H NMR (300 MHz, CDCl₃) δ 4.03 (q, J = 5.0 Hz, 2H), 4.18 (d, J = 3.0 Hz, 2H), 7.06 (d, J = 3.0 Hz, 2H), 7.87 (q, J = 8.0 Hz, 4H), 8.07 (d, J = 3.0 Hz, 2H). HRMS *m/z* C₁₆H₁₃N₂O₃I found 407.9983, calcd 407.9971 (M⁺).

4.1.8. 2-(2-(4-(5-(4-Iodophenyl)-1,3,4-oxadiazol-2-yl)phenoxy)ethoxy)ethanol (8)

The same reaction as described above to prepare **7** was used, and 9 mg of **8** was obtained in a 25.9% yield from **6** and ethylene glycol mono-2-chloroethyl ether. ¹H NMR (300 MHz, CDCl₃) δ 3.70 (t, J = 3.1 Hz, 2H), 3.79 (q, J = 4.8 Hz, 2H), 3.92 (t, J = 3.2 Hz, 2H), 4.23 (t, J = 3.1 Hz, 2H), 7.06 (d, J = 3.1 Hz, 2H), 7.87 (q, J = 7.6 Hz, 4H), 8.70 (d, J = 3.1 Hz, 2H). HRMS *m/z* C₁₈H₁₇N₂O₄I found 452.0244, calcd 452.0233 (M⁺).

4.1.9. 2-(2-(2-(4-(5-(4-Iodophenyl)-1,3,4-oxadiazol-2-yl)phenoxy)ethoxy)ethoxy)ethanol (9)

The same reaction as described above to prepare **7** was used, and 7.8 mg of **9** was obtained in a 44.7% yield from **6** and 2-[2-(chloroethoxy)ethoxy]ethanol. ¹H NMR (300 MHz, CDCl₃) δ 3.61–3.77 (m, 8H), 3.91 (t, J = 3.1 Hz), 4.23 (t, J = 3.2 Hz, 2H), 7.06 (d,

$J = 3.0$ Hz, 2H), 7.87 (q, $J = 7.8$ Hz, 4H), 8.06 (d, $J = 2.3$ Hz, 2H). HRMS m/z $C_{20}H_{21}N_2O_5$ found 496.0525, calcd 496.0495 (M^+).

4.2. Iododestannylation reaction

The radioiodinated forms of compounds **3** and **4** were prepared from the corresponding tributyltin derivatives by iododestannylation. Briefly, to initiate the reaction, 50 μ L of H_2O_2 (3%) was added to a mixture of a tributyltin derivative (50 μ g/50 μ L EtOH), [^{125}I]NaI (0.1–0.2 mCi, specific activity 2200 Ci/mmol), and 50 μ L of 1 N HCl in a sealed vial. The reaction was allowed to proceed at room temperature for 3 min and terminated by addition of NaHSO₃. After neutralization with sodium bicarbonate and extraction with ethyl acetate, the extract was dried by passing through an anhydrous Na₂SO₄ column and then blown dry with a stream of nitrogen gas. The radioiodinated ligand was purified by HPLC on a Cosmosil C₁₈ column with an isocratic solvent of H₂O/acetonitrile (4:6) at a flow rate of 1.0 mL/min.

4.3. Binding assays using the aggregated A β peptide in solution

A solid form of A β 42 was purchased from Peptide Institute (Osaka, Japan). Aggregation was carried out by gently dissolving the peptide (0.25 mg/mL) in a buffer solution (pH 7.4) containing 10 mM sodium phosphate and 1 mM EDTA. The solution was incubated at 37 °C for 42 h with gentle and constant shaking. Binding assays were carried out as described previously.²⁴ [^{125}I]IMPY (6-iodo-2-(4'-dimethylamino)phenyl-imidazo[1,2]pyridine) with 2200 Ci/mmol specific activity and greater than 95% radiochemical purity was prepared using the standard iododestannylation reaction as described previously.¹⁵ Binding assays were carried out in 12 \times 75 mm borosilicate glass tubes. A mixture containing 50 μ L of test compound (0.2 pM–400 μ M in 10% EtOH), 50 μ L of [^{125}I]IMPY (0.02 nM diluted in 10%EtOH), 50 μ L of A β 42 aggregates, and 850 μ L of 10% ethanol was incubated at room temperature for 3 h. The mixture was then filtered through Whatman GF/B filters using a Brandel M-24 cell harvester, and the filters containing the bound ^{125}I ligand were placed in a gamma counter (Aloka, ARC-380). Values for the half-maximal inhibitory concentration (IC₅₀) were determined from displacement curves of three independent experiments using GraphPad Prism 4.0, and those for the inhibition constant (K_i) were calculated using the Cheng–Prusoff equation.²⁵

4.4. Neuropathological staining of model mouse brain sections

The experiments with animals were conducted in accordance with our institutional guidelines and were approved by Nagasaki University Animal Care Committee. The Tg2576 transgenic mice (female, 28-month-old) and wild-type mice (female, 28-month-old) were used as the Alzheimer's model and control mice, respectively. After the mice were sacrificed by decapitation, the brains were immediately removed and frozen in powdered dry ice. The frozen blocks were sliced into serial sections, 10 μ m thick. Each slide was incubated with a 50% EtOH solution (100 μ M) of compounds **3** and **4** for 30 min. The sections were washed in 50% EtOH for 1 min two times, and examined using a microscope (Nikon Eclipse 80i) equipped with a UV-1A filter set (excitation, 365–375 nm; dichroic mirror, 400 nm; longpass filter, 400 nm). Thereafter, the serial sections were also stained with thioflavin S, a pathological dye commonly used for staining A β plaques in the brain, and examined using a microscope (Nikon Eclipse 80i) equipped with a B-2A filter set (excitation, 450–480 nm; dichroic mirror, 505 nm; longpass filter, 520 nm).

4.5. Determination of partition coefficient determination

Partition coefficients were measured by mixing [^{125}I]**3** and [^{125}I]**4** with 1.5 mL each of 1-octanol and buffer (0.1 M phosphate, pH 7.4) in a test tube. The test tube was vortexed for 20 s three times. Two weighed samples (1 mL each) from the 1-octanol and buffer layers were measured for radioactivity with a gamma counter. The partition coefficient was determined by calculating the ratio of cpm/1 mL of 1-octanol to that of the buffer.

4.6. In vivo biodistribution in normal mice

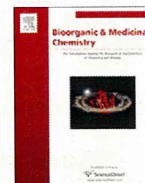
A saline solution (100 μ L) of radiolabeled agents (0.2–0.4 μ Ci) containing ethanol (10 μ L) was injected intravenously directly into the tail of ddY mice (5-week-old, 22–25 g). The mice were sacrificed at various time points postinjection. The organs of interest were removed and weighed, and radioactivity was measured with an automatic gamma counter (Aloka, ARC-380).

Acknowledgments

This study was supported by the Program for Promotion of Fundamental Studies in Health Sciences of the National Institute of Biomedical Innovation (NIBIO) and a Health Labour Sciences Research Grant.

References and notes

1. Klunk, W. E. *Neurobiol. Aging* **1998**, *19*, 145.
2. Hardy, J.; Selkoe, D. J. *Science* **2002**, *297*, 353.
3. Mathis, C. A.; Lopresti, B. J.; Klunk, W. E. *Nucl. Med. Biol.* **2007**, *34*, 809.
4. Mathis, C. A.; Wang, Y.; Klunk, W. E. *Curr. Pharm. Des.* **2004**, *10*, 1469.
5. Nordberg, A. *Lancet Neurol.* **2004**, *3*, 519.
6. Mathis, C. A.; Wang, Y.; Holt, D. P.; Huang, G. F.; Debnath, M. L.; Klunk, W. E. *J. Med. Chem.* **2003**, *46*, 2740.
7. Klunk, W. E.; Engler, H.; Nordberg, A.; Wang, Y.; Blomqvist, G.; Holt, D. P.; Bergstrom, M.; Savitcheva, I.; Huang, G. F.; Estrada, S.; Aussen, B.; Debnath, M. L.; Barletta, J.; Price, J. C.; Sandell, J.; Lopresti, B. J.; Wall, A.; Koivisto, P.; Antoni, G.; Mathis, C. A.; Langstrom, B. *Ann. Neurol.* **2004**, *55*, 306.
8. Ono, M.; Wilson, A.; Norbrega, J.; Westaway, D.; Verhoeff, P.; Zhuang, Z. P.; Kung, M. P.; Kung, H. F. *Nucl. Med. Biol.* **2003**, *30*, 565.
9. Verhoeff, N. P.; Wilson, A. A.; Takeshita, S.; Trop, L.; Hussey, D.; Singh, K.; Kung, H. F.; Kung, M. P.; Houle, S. *Am. J. Geriatr. Psychiatry* **2004**, *12*, 584.
10. Rowe, C. C.; Ackerman, U.; Browne, W.; Mulligan, R.; Pike, K. L.; O'Keefe, G.; Tochon-Danguy, H.; Chan, G.; Berlangieri, S. U.; Jones, G.; Dickinson-Rowe, K. L.; Kung, H. P.; Zhang, W.; Kung, M. P.; Skovronsky, D.; Dyrks, T.; Holl, G.; Krause, S.; Friebe, M.; Lehman, L.; Lindemann, S.; Dinkelborg, L. M.; Masters, C. L.; Villemagne, V. L. *Lancet Neurol.* **2008**, *7*, 129.
11. Kudo, Y.; Okamura, N.; Furumoto, S.; Tashiro, M.; Furukawa, K.; Maruyama, M.; Itoh, M.; Iwata, R.; Yanai, K.; Arai, H. *J. Nucl. Med.* **2007**, *48*, 553.
12. Agdeppa, E. D.; Kepe, V.; Liu, J.; Flores-Torres, S.; Satyamurthy, N.; Petric, A.; Cole, G. M.; Small, C. W.; Huang, S. C.; Barrio, J. R. *J. Neurosci.* **2001**, *21*, RC189.
13. Shoghi-Jadid, K.; Small, G. W.; Agdeppa, E. D.; Kepe, V.; Ercoli, L. M.; Siddarth, P.; Read, S.; Satyamurthy, N.; Petric, A.; Huang, S. C.; Barrio, J. R. *Am. J. Geriatr. Psychiatry* **2002**, *10*, 24.
14. Small, G. W.; Kepe, V.; Ercoli, L. M.; Siddarth, P.; Bookheimer, S. Y.; Miller, K. J.; Lavretsky, H.; Burggren, A. C.; Cole, G. M.; Vinters, H. V.; Thompson, P. M.; Huang, S. C.; Satyamurthy, N.; Phelps, M. E.; Barrio, J. R. *N. Engl. J. Med.* **2006**, *355*, 2652.
15. Kung, M. P.; Hou, C.; Zhuang, Z. P.; Zhang, B.; Skovronsky, D.; Trojanowski, J. Q.; Lee, V. M.; Kung, H. F. *Brain Res.* **2002**, *956*, 202.
16. Zhuang, Z. P.; Kung, M. P.; Wilson, A.; Lee, C. W.; Plossl, K.; Hou, C.; Holtzman, D. M.; Kung, H. F. *J. Med. Chem.* **2003**, *46*, 237.
17. Newberg, A. B.; Wintering, N. A.; Plossl, K.; Hochold, J.; Stabin, M. G.; Watson, M.; Skovronsky, D.; Clark, C. M.; Kung, M. P.; Kung, H. F. *J. Nucl. Med.* **2006**, *47*, 748.
18. Newberg, A. B.; Wintering, N. A.; Clark, C. M.; Plossl, K.; Skovronsky, D.; Seibyl, J. P.; Kung, M. P.; Kung, H. F. *J. Nucl. Med.* **2006**, *47*, 78.
19. Ono, M.; Haratake, M.; Saji, H.; Nakayama, M. *Bioorg. Med. Chem.* **2008**, *16*, 6867.
20. Neaterov, E. E.; Skoch, J.; Hyman, B. T.; Klunk, W. E.; Bacskai, B. J.; Swager, T. M. *Angew. Chem. Int. Ed.* **2005**, *44*, 5452.
21. Chabdra, R.; Kung, M. P.; Kung, H. F. *Bioorg. Med. Chem. Lett.* **2006**, *16*, 1350.
22. Qu, W.; Kung, M. P.; Hou, C.; Oya, S.; Kung, H. F. *J. Med. Chem.* **2007**, *50*, 3380.
23. Dabiti, M.; Salehi, P.; Baghbanzadeh, M.; Bahramnejad, M. *Tetrahedron Lett.* **2006**, *47*, 6983.
24. Kung, M. P.; Hou, C.; Zhuang, Z. P.; Skovronsky, D.; Kung, H. F. *Brain Res.* **2004**, *1025*, 98.
25. Cheng, Y.; Prusoff, W. H. *Biochem. Pharmacol.* **1973**, *22*, 3099.



Push–pull benzothiazole derivatives as probes for detecting β -amyloid plaques in Alzheimer's brains

Masahiro Ono^{a,*}, Shun Hayashi^{a,†}, Hiroyuki Kimura^a, Hidekazu Kawashima^b, Morio Nakayama^c, Hideo Saji^{a,*}

^a Graduate School of Pharmaceutical Sciences, Kyoto University, 46-29 Yoshida Shimoadachi-cho, Sakyo-ku, Kyoto 606-8501, Japan

^b Graduate School of Medicine, Kyoto University, Shogoin Kawahara-cho, Kyoto 606-8507, Japan

^c Graduate School of Biomedical Sciences, Nagasaki University, 1-14 Bunkyo-machi, Nagasaki 852-8521, Japan

ARTICLE INFO

Article history:

Received 29 June 2009

Revised 4 August 2009

Accepted 4 August 2009

Available online 20 August 2009

Keywords:

β -Amyloid

Push–pull dye

Imaging

Alzheimer's disease

ABSTRACT

We synthesized push–pull benzothiazole derivatives and evaluated their potential as β -amyloid imaging probes. In binding experiments *in vitro*, the benzothiazoles showed excellent affinity for synthetic $A\beta(1-42)$ aggregates. β -Amyloid plaques in the mouse and human brain were clearly visualized with the benzothiazoles, reflecting the results *in vitro*. These compounds may be a useful scaffold for the development of novel PET/SPECT and fluorescent tracers for detecting β -amyloid in Alzheimer's brains.

© 2009 Elsevier Ltd. All rights reserved.

1. Introduction

The formation of β -amyloid ($A\beta$) plaques is a key neurodegenerative event in Alzheimer's disease (AD).^{1,2} Since the imaging of these plaques *in vivo* may lead to the presymptomatic diagnosis of AD, many molecular probes for this purpose, including PET/SPECT and MRI tracers, have been developed.^{3–12} The PET ligand [¹¹C]-2-(4-(methylamino)phenyl)-6-hydroxybenzothiazole (6-OH-BTA-1 or PIB) with a benzothiazole backbone (Fig. 1) has shown particular promise in early clinical trials and is currently being used in a number of human studies.^{13–15} In addition to PET/SPECT and MRI probes, much attention has focused on the development of near-infrared fluorescent (NIRF) probes targeting $A\beta$ plaques.^{16–18} NIRF probes are typically small molecule fluorescent dyes designed to absorb and emit light in the near-infrared region, where tissue scattering and absorption is lowest. The simple synthesis, low-cost, and long shelf-life of NIRF probes, together with the low-cost of optical imaging devices, present an attractive alternative to MRI and PET/SPECT techniques.

Among NIRF probes reported, to date, NIAD crosses the blood–brain barrier, selectively binds $A\beta$ with high affinity, clears quickly

from the brain, and absorbs and emits within the near-infrared region (650–900 nm), often called the 'optical window' (Fig. 1).¹⁷ A series of NIAD derivatives have been designed and synthesized based on a classical push–pull architecture with terminal donor (hydroxy or dimethylamino group) and acceptor (dicyanomethylene group) moieties that are interconnected by a highly polarized bridge (dithienylethenyl group), because various donor and acceptor groups can be used to manipulate the relative energies of HOMO and LUMO and obtain the desired long wavelength of absorption/emission bands.¹⁷

On the basis of this approach to the molecular design, we planned to develop novel push–pull dyes for detecting $A\beta$ plaques in the brain. We selected benzothiazole or styrylbenzothiazole as the highly polarized bridge, a dimethylamino group as the donor, and a dicyanomethylene group as the acceptor. In the present study, we designed and synthesized two benzothiazole-derived push–pull dyes (PP-BTA-1 and PP-BTA-2 in Fig. 2), and evaluated their biological potential as probes for detecting $A\beta$ plaques in the brain. To our knowledge, this is the first time push–pull benzothiazole derivatives have been proposed as $A\beta$ imaging probes for detecting AD.

2. Results and discussion

The target benzothiazole derivatives were prepared as shown in Schemes 1 and 2. PP-BTA-1 (**4**) was successfully synthesized in a yield of 21.4% according to methods reported previously (Scheme

* Corresponding authors. Tel.: +81 75 753 4608; fax: +81 75 753 4568 (M.O), tel.: +81 75 753 4556; fax: +81 75 753 4568 (H.S.).

E-mail addresses: ono@pharm.kyoto-u.ac.jp (M. Ono), hsaji@pharm.kyoto-u.ac.jp (H. Saji).

[†] These authors contributed equally to this work.

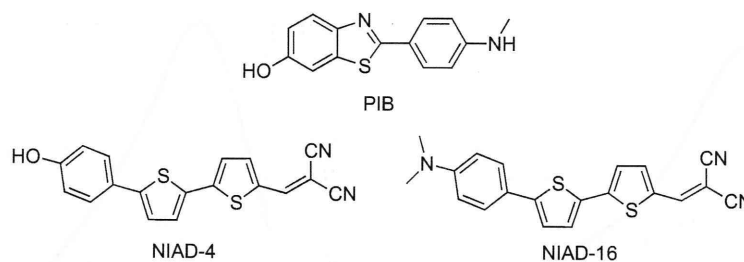


Figure 1. Chemical structures of PIB, NIAD-4 and NIAD-16.

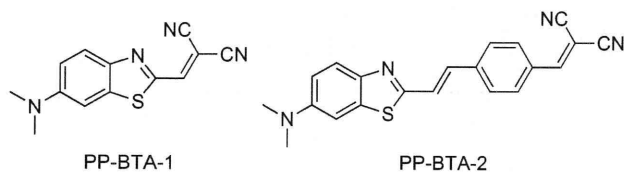


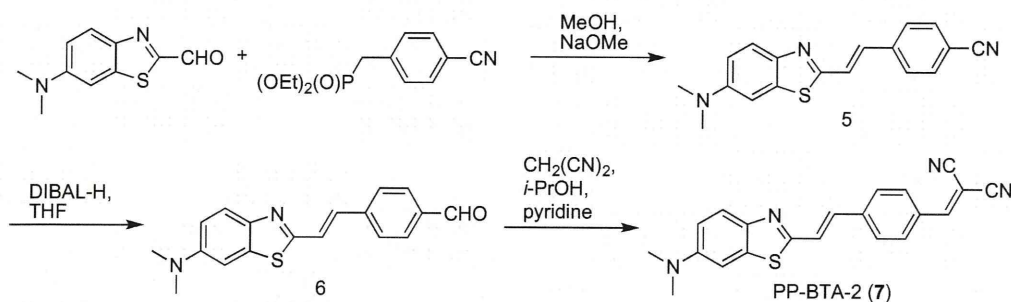
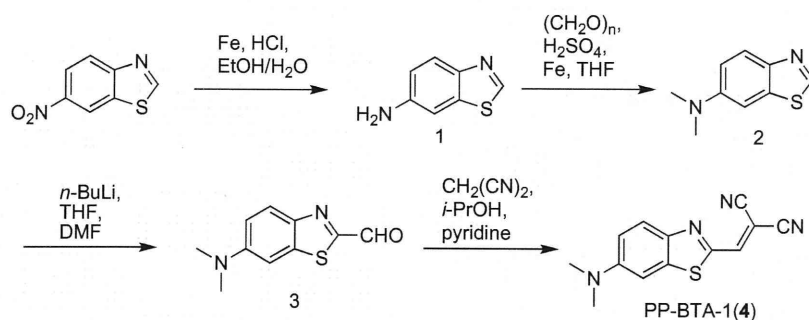
Figure 2. Chemical structures of push-pull benzothiazole derivatives reported in this paper.

1).¹⁹ The formation of styrylbenzothiazole in the synthesis of PP-BTA-2 (**7**) (Scheme 2) was achieved by a Wadsworth–Emmons reaction between diethyl (4-cyanobenzyl)phosphonate and 6-dimethylaminobenzothiazole-2-carbaldehyde. The desired (*E*)-styrylbenzothiazole derivative was prepared in a yield of 23.0%. The cyano group was converted to a formyl group by a reaction with DIBAL-H as reported.²⁰ The target PP-BTA-2 was prepared by the condensation of carbaldehyde with malononitrile.

NIRF imaging *in vivo* requires the development of new fluorescent compounds with optimal fluorescent properties and high affinity for A β plaques. First, we evaluated the fluorescent proper-

ties (absorption/emission wavelengths) of PP-BTA-1 and PP-BTA-2. PP-BTA-1 and PP-BTA-2 exhibited absorption/emission peaks at 540/634 nm and 410/529 nm in EtOH, respectively. The extension of π -conjugation generally leads to absorption/emission bands with longer wavelengths. However, PP-BTA-2 showed a shorter wavelength than PP-BTA-1 despite a longer π -conjugation. On the other hand, because the wavelength of PP-BTA-1 is close to the near-infrared region, a slight modification should lead to a wavelength appropriate for imaging *in vivo*. Furthermore, when PP-BTA-1 and PP-BTA-2 existed in a solution containing A β (1–42) aggregates, the fluorescence intensity of PP-BTA-1 and PP-BTA-2 increased with the concentration of A β (1–42) aggregates, indicating affinity for A β aggregates (Fig. 3).

To quantify the affinity of push-pull benzothiazole derivatives for A β plaques, we carried out inhibition assays on the binding to A β (1–42) aggregates with thioflavin T as a competing ligand. PP-BTA-1 and PP-BTA-2 displaced thioflavin T in a dose-dependent manner, indicating that they have affinity for A β (1–42) aggregates (Fig. 4). In addition, this result suggests that PP-BTA-1 and PP-BTA-2 may occupy a binding site on A β aggregates similar to that of thioflavin T. The apparent IC₅₀ values for PP-BTA-1, PP-BTA-2 and PIB were 0.12, 0.11 and 0.67 μ M, respectively (Table 1). The IC₅₀ of



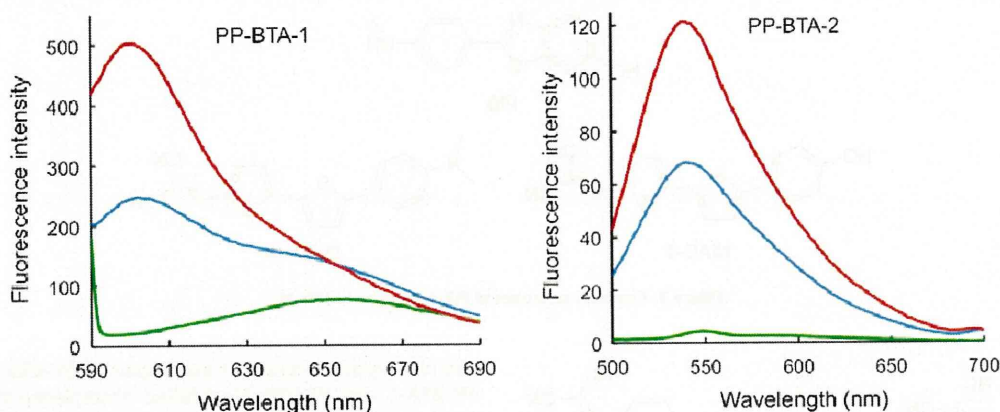


Figure 3. A β -dependent change in the fluorescence spectra of PP-BTA-1 and PP-BTA-2. Green, blue and red lines show the fluorescence spectrum of 0, 5 and 10 μ g/mL of A β (1-42) aggregates, respectively.

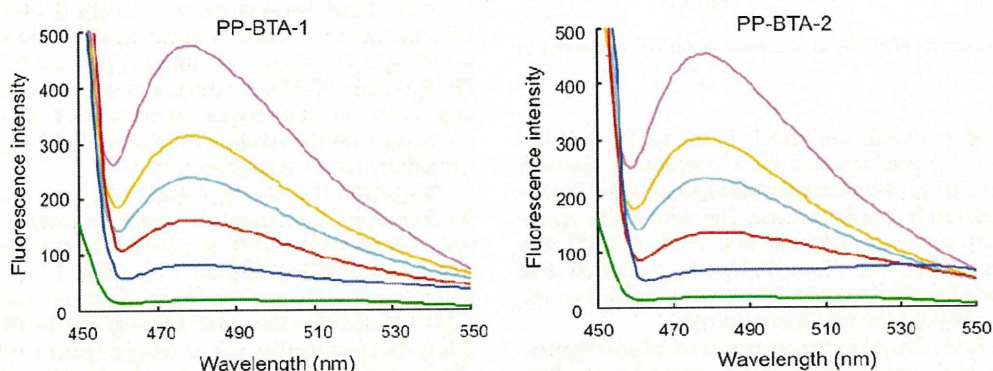


Figure 4. Inhibition assays of PP-BTA-1 and PP-BTA-2 using thioflavin T as the ligand in A β (1-42) aggregates. Fluorescence spectral change of thioflavin T (3 μ M) upon addition of 0.0611 (orange line), 0.122 (cyan line), 0.486 (red line), or 2.65 (blue line) μ M of PP-BTA-1 and PP-BTA-2 to A β (1-42) aggregates (10 μ g/mL). A pink line shows the fluorescence spectrum of thioflavin T (3 μ M) with A β (1-42) aggregates. A green line shows the fluorescence spectrum of thioflavin T (3 μ M) alone.

Table 1

Apparent inhibition constants (IC_{50} , μ M) of benzothiazoles for the binding of thioflavin T to A β (1-42) aggregates

Compound	IC_{50}^a (μ M)
PP-BTA-1 (4)	0.12 ± 0.001
PP-BTA-2 (7)	0.11 ± 0.001
PIB	0.67 ± 0.11

^a Each value represents the mean \pm standard error of the mean for three independent experiments.

PP-BTA-1 and PP-BTA-2 was lower than that of PIB, which is commonly used for clinical research, indicating PP-BTA-1 and PP-BTA-2 to have greater affinity for A β (1-42) aggregates. While PP-BTA-1 does not have the phenyl group in the phenylbenzothiazole structure that PIB possesses, it showed stronger binding to A β aggregates than PIB. Moreover, benzothiazole is a compact molecule advantageous for penetration of the blood–brain barrier after administration in vivo. These results suggest benzothiazole to be a useful scaffold for the development of A β imaging agents in vivo.

Next, the usefulness of PP-BTA-1 and PP-BTA-2 for neuropathological staining of A β plaques was investigated in an animal model of AD, the Tg2576 mouse, specifically engineered to overproduce A β plaques in the brain. PP-BTA-1 and PP-BTA-2 clearly stained the plaques as reflected by the high affinity for A β aggregates in in vitro competition assays (Fig. 5). The labeling pattern was consistent with that observed with thioflavin S. In contrast, wild-

type mice displayed no remarkable accumulation of PP-BTA-1 and PP-BTA-2 in brain sections. These results suggest that PP-BTA-1 and PP-BTA-2 show affinity for A β plaques in the mouse brain in addition to having affinity for synthetic A β (1-42) aggregates.

Furthermore, we also investigated the effectiveness of PP-BTA-1 and PP-BTA-2 for neuropathological staining of A β plaques in human AD brain sections (Fig. 6). A previous report suggested the configuration/folding of A β plaques in Tg2576 mice to be different from the tertiary/quaternary structure of A β plaques in AD brains.²¹ Therefore, it is important to evaluate the binding affinity for A β plaques in human AD brains. PP-BTA-1 and PP-BTA-2 clearly stained many neuritic plaques in AD brains (Fig. 6A and D). In contrast, no apparent staining was observed in adult normal brain sections (Fig. 6C and F). The labeling pattern was consistent with that observed by immunohistochemical labeling with an antibody specific to A β (Fig. 6B and E), indicating that PP-BTA-1 and PP-BTA-2 may be applicable for in vivo imaging of A β plaques in Alzheimer's brains and deserve further investigation as a potential tool for early diagnosis.

Since PP-BTA-1 and PP-BTA-2 possess a dimethylamino group, they can be used as probes for PET by labeling one of two methyl groups with ¹¹C. In addition, for the application of push–pull benzothiazole derivatives to optical imaging in vivo, the fine-tuning of absorption/emission wavelengths to a desired region continues by optimizing the combination of donor and acceptor groups.

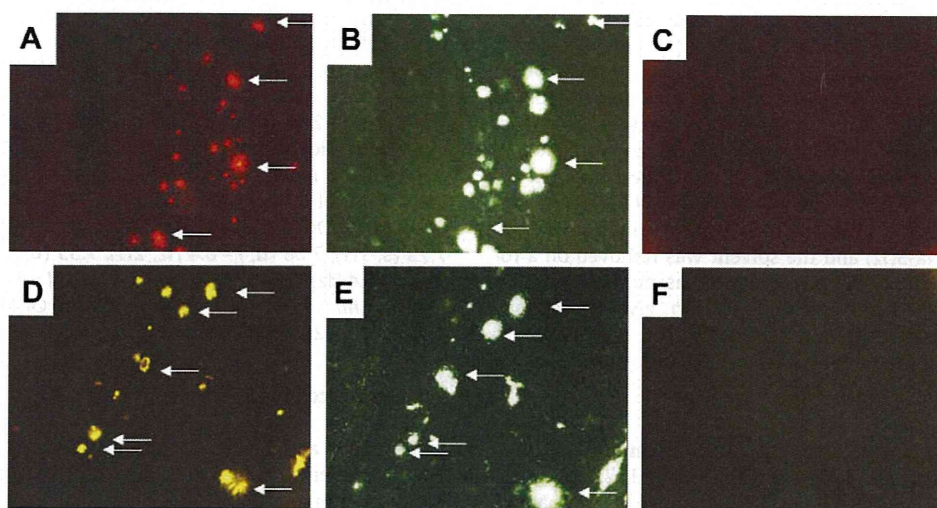


Figure 5. Neuropathological staining of PP-BTA-1 and PP-BTA-2 in 10 μm sections from a mouse model of AD (A and D) and a wild-type mouse (C and F). A β plaques labeled with PP-BTA-1 and PP-BTA-2 were confirmed by staining of the serial sections using thioflavin S (B and E).

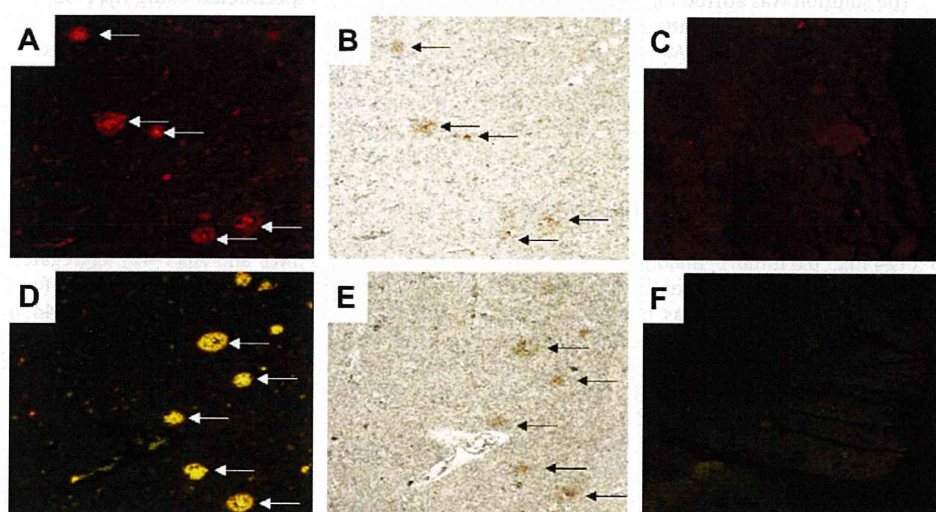


Figure 6. Neuropathological staining of 5 μm AD brain sections from the temporal cortex (A, B, D and E) and adult normal temporal brain sections (C and F). Many neuritic plaques are clearly stained with PP-BTA-1 (A) and PP-BTA-2 (D). Intense fluorescence can be seen in the core of neuritic plaques. A β immunostaining with anti A β antibodies in the serial sections shows an identical staining pattern of plaques (B and E). No apparent staining was observed in adult normal brain sections (C and F).

3. Conclusion

In conclusion, we successfully designed and synthesized benzothiazole-derived push-pull dyes for imaging A β plaques in the brain. In binding experiments *in vitro*, these benzothiazole compounds showed high affinity for A β (1–42) aggregates. PP-BTA-1 and PP-BTA-2 clearly stained A β plaques in both mouse brain and human brain, reflecting their affinity for A β aggregates *in vitro*. These findings suggest that additional structural changes on the benzothiazole backbone may be applied to potential A β probes for not only optical imaging but also PET and SPECT.

4. Experimental

^1H NMR spectra were obtained on a JEOL JNM-LM400 with TMS as an internal standard. Coupling constants are reported in hertz. Multiplicity was defined by s (singlet), d (doublet), t (triplet), br (broad) and m (multiplet). Mass spectra were obtained on a SHIMADZU LCMS-2010 EV. PIB was purchased from ABX (Radeberg,

Germany). Other reagents were of reagent grade and used without further purification unless otherwise indicated.

4.1. Chemistry

4.1.1. 1,3-Benzothiazol-6-amine (1)

To a mixture of 6-nitrobenzothiazole (2.5 g, 13.9 mmol) and concentrated HCl (1.93 mL, 22.7 mmol) in 80% EtOH (63 mL) was added powdered iron (3.7 g, 55.6 mmol). The reaction mixture was stirred for 1 h under reflux, and then cooled to room temperature. The precipitate of iron oxides and hydroxy salts was removed by filtration. The solvent was removed and the solid residue was extracted into a heterogeneous mixture of EtOAc (50 mL \times 2) and a 10% aqueous solution of Na $_2$ CO $_3$ (50 mL). The EtOAc extract was dried (Na $_2$ SO $_4$) and the solvent was removed under vacuum to yield **1** (1.91 g, 91.7%). ^1H NMR (400 MHz, CDCl $_3$) δ 8.70 (s, 1H), 7.89 (d, J = 8.8 Hz, 1H), 7.17 (d, J = 2.4 Hz, 1H), 6.87 (dd, J = 8.8, 2.4 Hz, 1H), 3.85 (br s, 2H). MS m/z 151 [MH $^+$].

4.1.2. *N,N*-Dimethyl-1,3-benzothiazol-6-amine (2)

A solution of **1** (1.47 g, 9.8 mmol) in THF (40 mL) was slowly added to a stirred mixture of 40% aqueous formaldehyde (7.24 mL, 98 mmol) and 4 M H₂SO₄ (7.95 mL, 29.4 mL). Powdered iron (4.36 g, 78.4 mL) was then added and the mixture was vigorously stirred for 3 h. The precipitate of iron salts was removed by filtration and washed with EtOAc (20 mL × 2). The combined organic solutions were made strongly basic with 1 N NaOH (50 mL) and extracted with EtOAc (50 mL × 2). The combined EtOAc extracts were dried (Na₂SO₄) and the solvent was removed on a rotary vacuum evaporator. The oily residue was purified by silica gel chromatography (hexane/EtOAc = 4:1) to give **2** (460 mg, 26.3%). ¹H NMR (400 MHz, CDCl₃) δ 8.67 (s, 1H), 7.95 (d, *J* = 8.8 Hz, 1H), 7.15 (d, *J* = 2.4 Hz, 1H), 7.00 (dd, *J* = 8.8, 2.4 Hz, 1H), 3.04 (s, 6H). MS *m/z* 179 [MH⁺].

4.1.3. 6-(Dimethylamino)-1,3-benzothiazole-2-carbaldehyde (3)

To a vigorously stirred solution of *n*-BuLi (0.5 mL, 2.6 M in hexane, 1.3 mmol) in THF (5.8 mL) at –78 °C under N₂ was added slowly a solution of **2** (220 mg, 1.23 mmol). The reaction mixture was stirred, warmed to –50 °C and after 1 h cooled to –78 °C. To the resulting solution of aryllithium salt was added slowly anhydrous DMF (0.38 mL). The solution was stirred for 2 h, poured into H₂O (9 mL), neutralized with an aqueous saturated solution of NH₄Cl and subsequently extracted with EtOAc (20 mL × 2). The combined extracts were dried over Na₂SO₄ and the solvent was removed under vacuum to give **3** (255 mg, 97.3%). ¹H NMR (400 MHz, CDCl₃) δ 10.06 (s, 1H), 8.03 (d, *J* = 10.0 Hz, 1H), 7.07–7.04 (m, 2H), 3.12 (s, 6H). MS *m/z* 207 [MH⁺].

4.1.4. ((6-(Dimethylamino)-1,3-benzothiazol-2-yl)methylene)malononitrile (PP-BTA-1, 4)

A solution of **3** (124 mg, 0.6 mmol), malononitrile (60 mg, 0.9 mmol) and pyridine (0.12 mL) in 2-propanol (7.2 mL) was stirred and refluxed for 30 min. The mixture was poured into H₂O (20 mL) and extracted with CHCl₃ (20 mL × 3). The combined extracts were dried over Na₂SO₄ and the solvent was removed under vacuum to give **4** (152 mg, 91.7%). ¹H NMR (400 MHz, CDCl₃) δ 7.99 (s, 1H), 7.99 (d, *J* = 9.2 Hz, 1H), 7.08 (dd, *J* = 9.2, 2.4 Hz, 1H), 7.02 (d, *J* = 2.4 Hz, 1H), 3.16 (s, 6H). MS *m/z* 255 [MH⁺]. Anal. Calcd for C₁₃H₁₀N₄S: C, 61.40; H, 3.96; N, 22.03; S, 12.61. Found: C, 61.34; H, 3.84; N, 21.82; S, 12.64.

4.1.5. 4-((*E*)-2-(6-(Dimethylamino)-1,3-benzothiazol-2-yl)vinyl)benzonitrile (5)

To a solution of (4-cyanobenzyl)phosphonate (403.6 mg, 1.6 mmol) in MeOH (12.8 mL) was added NaOMe (0.632 mL). The mixture was cooled in an ice bath, and stirred under reflux for 3 h after the addition of **3** (330 mg, 1.6 mmol). The solid that formed in the reaction mixture was filtered to give **5** (385 mg, 78.8%). ¹H NMR (400 MHz, CDCl₃) δ 7.84 (d, *J* = 9.6 Hz, 1H), 7.64 (dd, *J* = 21.2, 8.0 Hz, 4H), 7.45 (d, *J* = 16.4 Hz, 1H), 7.32 (d, *J* = 16.4 Hz, 1H), 7.06 (d, *J* = 2.8 Hz, 1H), 6.95 (dd, *J* = 9.6, 2.8 Hz, 1H), 3.06 (s, 6H). MS *m/z* 306 [MH⁺].

4.1.6. 4-((*E*)-2-(6-(Dimethylamino)-1,3-benzothiazol-2-yl)vinyl)benzaldehyde (6)

To a solution of **5** (61 mg, 0.2 mmol) in THF (3.3 mL) was added DIBAL-H (1 M in hexane, 0.5 mL) at –78 °C. The reaction mixture was stirred at room temperature overnight. Thereafter, 10% acetic acid (15 mL) was added and the mixture was extracted with CHCl₃ (20 mL × 2). After the organic layer was washed with saline, the combined extracts were dried over Na₂SO₄. The residue was purified by silica gel chromatography (hexane/EtOAc = 2:1) to give **6** (28 mg, 45.4%). ¹H NMR (400 MHz, CDCl₃) δ 10.02 (s, 1H), 7.90 (d, *J* = 8.4 Hz,

2H), 7.85 (d, *J* = 8.2 Hz, 1H), 7.67 (d, *J* = 8.4 Hz, 2H), 7.50 (d, *J* = 16.4 Hz, 1H), 7.38 (d, *J* = 16.4 Hz, 1H), 7.07 (d, *J* = 2.4 Hz, 1H), 6.96 (dd, *J* = 8.8, 2.4 Hz, 1H), 3.06 (s, 6H). MS *m/z* 309 [MH⁺].

4.1.7. 4-((*E*)-2-(6-(Dimethylamino)-1,3-benzothiazol-2-yl)vinyl)benzylidene)malononitrile (PP-BTA-2, 7)

The same reaction as described above to prepare **5** was used, and 45 mg of **7** was obtained in a 63.5% yield from **6**. ¹H NMR (400 MHz, CDCl₃) δ 7.94 (d, *J* = 8.4 Hz, 2H), 7.86 (d, *J* = 8.8 Hz, 1H), 7.73 (s, 1H), 7.68 (d, *J* = 8.4 Hz, 2H), 7.53 (d, *J* = 16.4 Hz, 1H), 7.35 (d, *J* = 16.4 Hz, 1H), 7.08 (s, 1H), 6.97 (d, *J* = 10.0 Hz, 1H), 3.08 (s, 6H). MS *m/z* 357 [MH⁺]. Anal. Calcd for C₂₇H₁₆N₄S: C, 70.76; H, 4.52; N, 15.72; S, 9.00. Found: C, 70.48; H, 4.57; N, 15.43; S, 8.99.

4.2. Fluorescence experiments

PP-BTA-1 and PP-BTA-2 were dissolved in 5% EtOH at 10 μM. The fluorescence of PP-BTA-1 and PP-BTA-2 was measured with a spectrophotometer (RF-1500, Shimadzu, Japan). For some measurements, the spectra of PP-BTA-1 and PP-BTA-2 were determined with or without Aβ(1–42) aggregates (0, 5 and 10 μM).

4.3. Binding experiments using Aβ(1–42) aggregates

A solid form of Aβ(1–42) was purchased from Peptide Institute (Osaka, Japan). Aggregation was carried out by gently dissolving the peptide (0.25 mg/mL) in a buffer solution (pH 7.4) containing 10 mM sodium phosphate and 1 mM EDTA. The solution was incubated at 37 °C for 42 h with gentle and constant shaking. Thioflavin-T was used as the tracer for the competition binding experiments. A mixture (3.6 mL of 10% EtOH) containing PP-BTA-1, PP-BTA-2 and PIB (final concn 61.1 nM–5.48 μM), thioflavin-T (final concn 3 μM), and Aβ(1–42) aggregates (final concn 10 μg/mL) was incubated at room temperature for 10 min. Fluorescence intensity at an excitation wavelength of 445 nm was plotted, and values for the apparent half-maximal inhibitory concentration (IC₅₀) were determined from a calibration curve of fluorescence intensity at 478 nm in three independent experiments.

4.4. Staining of Aβ plaques in Tg2576 mouse brain sections

The experiments with animals were conducted in accordance with our institutional guidelines and approved by the Kyoto University Animal Care Committee. The Tg2576 transgenic mice (female, 27-month-old) and wild-type mice (female, 27-month-old) were used as the Alzheimer's model and control mice, respectively. After the mice were sacrificed by decapitation, the brains were immediately removed and frozen in powdered dry ice. The frozen blocks were sliced into serial sections, 10 μm thick. Each slide was incubated with a 50% EtOH solution (100 μM) of PP-BTA-1 and PP-BTA-2 for 10 min. The sections were washed in 50% EtOH for 1 min two times, and examined using a microscope (Nikon Eclipse 80i) equipped with a G-2A filter set (excitation, 510–560 nm; dichroic mirror, 575 nm; longpass filter, 470 nm) for PP-BTA-1, and a B-2A filter set (excitation, 450–480 nm; dichroic mirror, 505 nm; longpass filter, 520 nm) for PP-BTA-2. Thereafter, the serial sections were also stained with thioflavin S, a pathological dye commonly used for staining Aβ plaques in the brain, and examined using a microscope (Nikon Eclipse 80i) equipped with a BV-2A filter set (excitation, 400–440 nm; dichroic mirror, 455 nm; longpass filter, 470 nm).

4.5. Staining of Aβ plaques in human AD brain sections

Postmortem brain tissues from an autopsy-confirmed case of AD (73-year-old male) and a control subject (36-year-old male) were